OPEN ACCESS

Energy Storage REVIEW

The Innovation Energy

Electrolyte architecture as the unifying design principle for hybrid solid polymer electrolytes

Anagipura Tharika Gimhani,[1,2] Muhammad Muzakir,[1,2] Shanmin Wang,[3] Prasit Pattananuwat,[2] Manunya Okhawilai,[4] and Jiaqian Qin[2,5,*]

*Correspondence: Jiaqian.Q@chula.ac.th

Received: March 26, 2026; Accepted: June 17, 2026; Published Online: July 22, 2026; https://doi.org/10.59717/j.xinn-energy.2026.100168

GRAPHICAL ABSTRACT

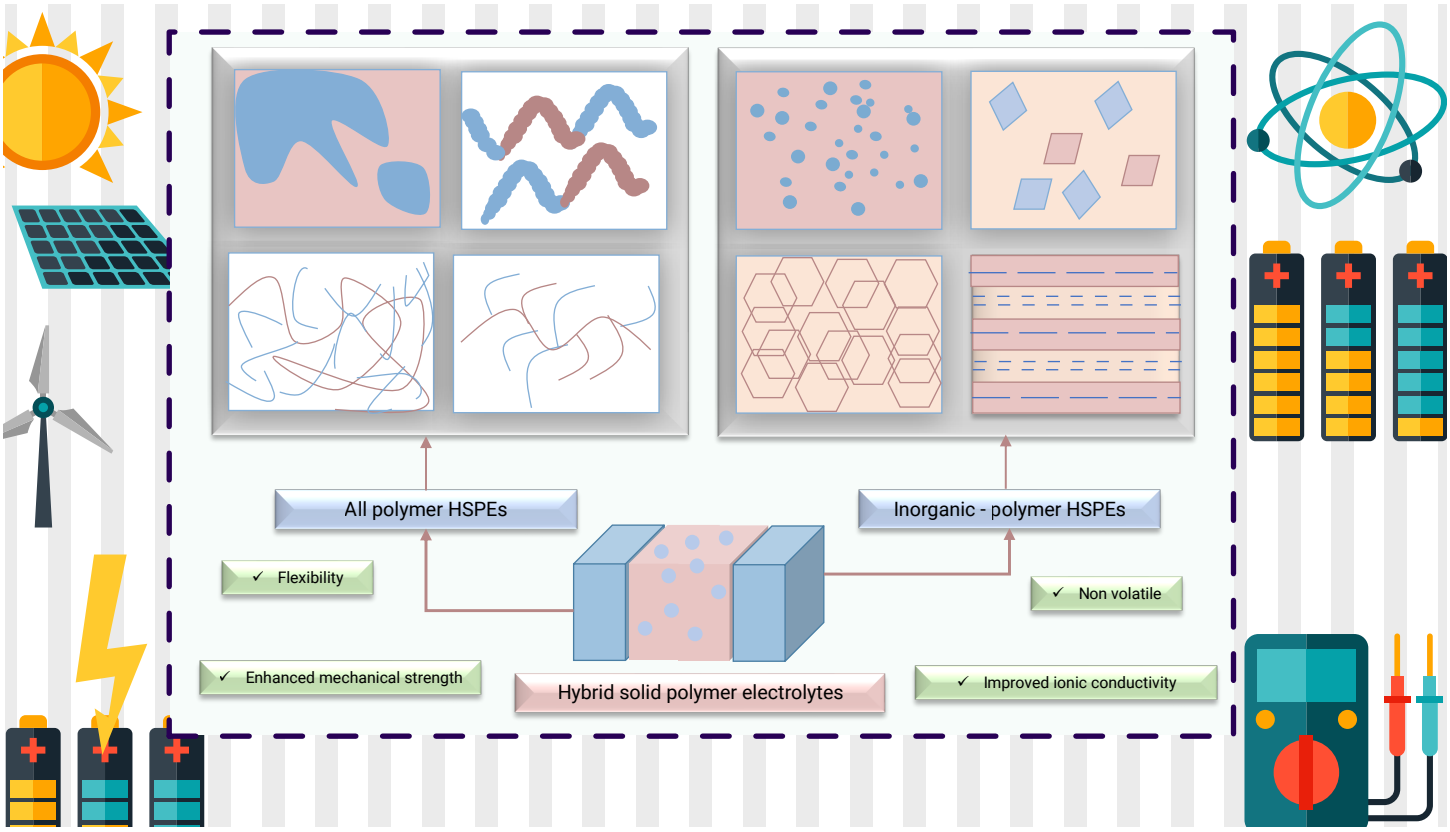

PUBLIC SUMMARY

- Hybrid solid polymer electrolytes (HSPEs) balance mechanical, processing and conductive properties, vital for high-performance solid-state lithium batteries.
- An architecture-centered classification divides HSPEs into phase-engineered polymer and polymer-inorganic network-engineered structural systems.
- Ion conduction of two HSPE categories is controlled by phase compatibility or ceramic network connectivity/tortuosity respectively.
- This structural classification clarifies structure-transport-performance relations beyond simple material-based sorting.
- Multiscale design and data-driven screening are promising routes to safe, high-energy-density solid-state batteries with optimized HSPEs.

REVIEW Energy Storage

www.the-innovation.org/the-innovation-energy

Electrolyte architecture as the unifying design principle for hybrid solid polymer electrolytes

Anagipura Tharika Gimhani,[1,2] Muhammad Muzakir,[1,2] Shanmin Wang,[3] Prasit Pattananuwat,[2] Manunya Okhawilai,[4] and Jiaqian Qin[2,5,*]

[1]International Graduate Program of Nanoscience and Technology, College of Interdisciplinary and Integrative Studies, Chulalongkorn University, Bangkok 10330, Thailand
[2]Center of Excellence on Advanced Materials for Energy Storage, Department of Materials Science, Faculty of Science, Chulalongkorn University, Bangkok 10330, Thailand
[3]Department of Physics, Southern University of Science and Technology, Shenzhen, Guangdong 518055, China
[4]Department of Chemical Engineering, Faculty of Engineering, Chulalongkorn University, Bangkok 10330, Thailand
[5]Energy Research Institute, Chulalongkorn University, Bangkok 10330, Thailand
*Correspondence: Jiaqian.Q@chula.ac.th

Received: March 26, 2026; Accepted: June 17, 2026; Published Online: July 22, 2026; https://doi.org/10.59717/j.xinn-energy.2026.100168

Citation: Gimhani A., Muzakir M., Wang S., et al. (2026). Electrolyte architecture as the unifying design principle for hybrid solid polymer electrolytes. *The Innovation Energy* 3:100168.

Hybrid solid polymer electrolytes (HSPEs) are central to advancing solid-state lithium batteries, offering a balance of mechanical integrity, processability, and ionic conductivity. This review introduces an architecture-based classification that unifies diverse HSPE designs by explicitly linking structural motifs to ion transport pathways. Two principal paradigms are defined: phase-engineered polymer architectures, encompassing miscible and immiscible blends, block copolymers, graft copolymers, and interpenetrating polymer networks, where phase continuity and interfacial compatibility govern transport; and network engineered polymer–inorganic architectures, including particulate composites, percolated one and two dimensional frameworks, continuous three-dimensional ceramic scaffolds, and layered or graded laminates, where network tortuosity and connectivity shape conduction. By framing HSPEs through architectural principles rather than material categories, this perspective establishes a clear structure–transport–performance relationship. Emerging directions in multiscale design and data-driven discovery are highlighted as pathways to safe, high-energy solid-state batteries. This architectural lens provides rational guidelines for bridging fundamental ionic with the stringent requirements of next-generation energy storage.

INTRODUCTION

The growing demand for high energy, safe, and durable storage systems for electric vehicles, portable electronics, and renewable integration has positioned lithium batteries at the center of advanced energy research. Electrolytes are pivotal, governing ionic transport, electrochemical stability, and thermal safety. Conventional systems fall into three categories:

• Liquid electrolytes (e.g., $LiPF_6$ or LiTFSI in carbonate solvents) provide high ionic conductivity (~10^{-2} S cm^{-1}) and facile processing but suffer from flammability, limited voltage stability (< 4.3 V vs. Li/Li^+), and dendrite risks.[1-2]

• Inorganic solid electrolytes (oxide, sulfide, and halide families) can reach comparable conductivities and offer wide stability windows, yet are constrained by brittleness, processing complexity, and high interfacial resistance.[3]

• Polymer electrolytes such as PEO–LiTFSI or PVDF-HFP blends offer flexibility and interfacial tunability but exhibit low ambient conductivity (10^{-7}–10^{-6} S cm^{-1}) and limited oxidative stability without modification.[4-5]

While solid electrolytes mitigate flammability and enable lithium metal (3860 mAh g^{-1}, −3.04 V vs. SHE) by suppressing dendrites,[6,7,8,9] conventional solid polymer electrolytes (SPEs) remain limited by poor room temperature conductivity,[10] insufficient modulus, narrow electrochemical windows, and unstable electrode interface.[11] These tradeoffs highlight the need for architectures that simultaneously optimize transport, mechanics, and interfacial compatibility.

HSPEs have therefore attracted rapidly increasing attention. By integrating inorganic phases (e.g., garnet, NASICON,[12] perovskites[13]) within polymer matrices, HSPEs combine polymer processability with ceramic conductivity and stiffness. Parallel to these inorganic systems, advanced crystalline organic frameworks such as covalent organic frameworks (COFs)[2] and furan based COFs (F-COFs)[5] have also gained traction in battery research, functioning either as ordered ion conducting channels in electrolytes or as conductive matrices in electrodes.[14] However, such designs enhance ambient ionic conductivity, reinforce mechanical strength, mitigate dendrite growth,[15] expand electrochemical stability, and reduce interfacial resistance.[16] Their flexibility and scalable processing further support practical manufacturing and cycling durability,[17] while offering improved safety and sustainability relative to liquid systems.[18]

Despite extensive publications, the HSPEs field remains conceptually fragmented. All polymer hybrids are typically classified by polymer chemistry or segmental dynamics,[19,20,21] whereas polymer–inorganic systems are organized by filler chemistry (e.g., NASICON [12]), active vs. inactive fillers,[22,23] dimensionality,[24,25] specific transport mechanisms,[26] or often as a discussion within a single host such as PEO.[27,28] This material centric taxonomy obscures the governing role of mesoscale structure. Current schemes based on composition, salt choice, or interfacial modification[23] do not systematically correlate electrolyte topology with ion transport kinetics. Consequently, systems with fundamentally different spatial organizations are frequently evaluated under similar descriptors, limiting predictive design.

Here, we propose electrolyte architecture as the unifying design principle for HSPEs. We introduce an architecture driven framework that transcends material boundaries by classifying HSPEs into two overarching paradigms: (i) phase engineered polymer architectures (All Polymer HSPEs) , including miscible/immiscible blends, block and graft copolymers, and interpenetrating networks and (ii) network engineered architectures (Polymer-Inorganic HSPEs), spanning particulate composites, percolated 1D/2D networks, continuous 3D ceramic scaffolds, and layered or graded laminates. Unlike traditional empirical approaches, this framework treats topological parameters such as the scale of phase continuity, interfacial thickness, and the percolation threshold as primary design variables. By quantifying how these geometric features dictate lithium-ion transport pathways and charge distribution at heterojunctions, we establish a predictive structure–architecture–performance paradigm. This approach enables the optimization of macroscopic metrics, including ionic conductivity (σ) and lithium transference number (t_{Li^+}), moving toward the topology driven design of durable, high-energy solid-state lithium batteries.

CLASSIFICATION OF HSPES

Phase engineered polymer architectures (all polymer HSPEs)

All polymer HSPEs integrate two or more polymer phases to surpass single component systems in ionic transport, mechanical strength, thermal stability and electrode compatibility. In these systems, performance is derived entirely from macromolecular architecture the spatial arrangement and connectivity of chemically distinct domains rather than inorganic reinforcement. The efficacy of these architectures is governed by several key topological parameters that establish the structure-property-performance relationship:

• Percolation Threshold: The critical volume fraction required for the ion-solvating phase to form a continuous 3D network. Architectural control aims to minimize percolation threshold to maintain high conductivity at low loading of the soft phase.

• Tortuosity (τ): The ratio of the actual ion path length to the geometric thickness. While random blends may suffer from high τ, ordered architectures provide streamlined pathways that maximize the effective diffusion coefficient.

• Interfacial Thickness and Energy: The characteristics of the phase

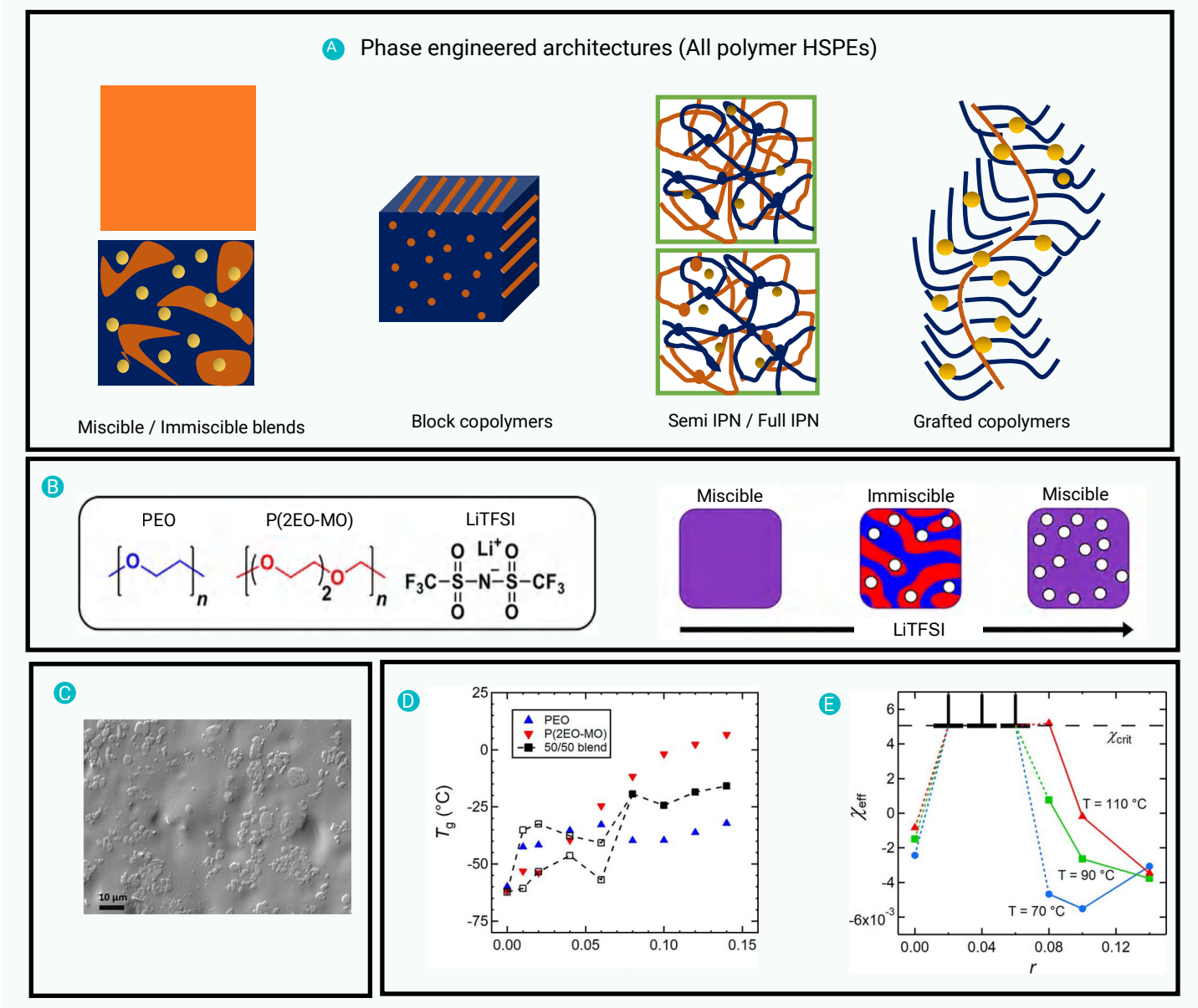

Figure 1. (A) Phase engineered polymer architecture. Redrawn and modified from Ref.[29,21,30]. (B) Effect of LiTFSI addition to PEO/P(2EO-MO) blend. Reproduced with permission from Ref.[29]. Copyright © 2020, American Chemical Society. SEM micrographs of (C) Immiscible blend SPE (50/50 vol% PPC/PVA and 24.5 wt.% LiTFSI salt). Reproduced with permission from Ref.[31]. Copyright © 2021 American Chemical Society. (D) T_g as a function of salt concentration, r, for each conventional polymer electrolyte system (solid blue triangles for PEO (Mn = 100 kg mol^{-1}) and solid red triangles for P(2EO-MO) (Mn = 55.2 kg mol^{-1})) and the polymer blend electrolyte. (E) Effective Flory Huggins interaction parameter, χ_{eff}, for the dPEO/P(2EO-MO)/LiTFSI (P(2EO -MO) Mn = 26.7 kg mol^{-1}) blends as a function of salt concentration, r, at three different temperatures: 70 °C (blue circles), 90 °C (green squares), and 110 °C (red triangles). Reproduced with permission from Ref.[29]. Copyright © 2020, American Chemical Society.

boundaries dictate both the interfacial resistance to ion hopping and the mechanical load transfer between the rigid and conductive phases.

Typically, one phase reduces glass transition temperature (T_g) and suppresses crystallinity to provide ion solvation, while a mechanically robust or crosslinked counterpart ensures modulus and resistance to dendrite growth. As shown in Figure 1A, these systems are classified as blends, block copolymers, interpenetrating networks, and graft copolymers based on how these topological parameters are engineered to decouple transport from mechanical integrity (Table 1).

Miscible and immiscible blends. Polymer blends in solid electrolytes are categorized as miscible or immiscible according to their phase architecture. Miscible systems form a homogeneous single phase with one T_g, whereas immiscible blends (Figure 1C) generate heterogeneous dual phase morphology with two T_g. This architectural distinction dictates ion transport by regulating the continuity of solvating domains and polar group distribution. Phase behavior is governed by the Flory Huggins interaction parameter χ , degree of polymerization, and processing conditions.[31,19] In classical Flory Huggins theory, the free energy of mixing per unit volume of a salt free binary polymer blend is given by[32]

$$v\frac{\Delta G_m}{k_B T} = \phi_{polymer}\left(\frac{\phi_A \ln \phi_A}{N_A} + \frac{\phi_B \ln \phi_B}{N_B} + \chi \phi_A \phi_B\right),$$

where v is a reference volume, φ_i and N_i are the volume fraction and degree of polymerization of component i, and χ is an interaction parameter that reflects the energetic preference for unlike contacts. Negative or small χ values favor miscibility, whereas larger positive values promote phase separation. When lithium salts are introduced, salt–polymer interactions and ion solvation modify the effective interaction parameter χ_{eff}, which can be expressed in the same formalism by replacing χ with χ_{eff}.[29,32] Solvated ions often reduce χ_{eff} and can drive a transition from immiscible to miscible behavior as salt concentration increases (Figure 1B).

T_g serves as a practical indicator of miscibility. Miscible blends show a single T_g, whereas immiscible blends show two distinct transitions associated with each polymer (Figure 1D). In PEO/P(2EO–MO) electrolytes, Gao and

Table 1. Summary of phase engineered polymer architectures: all polymer HSPEs

Polymer matrix	Electrolyte composition	Ionic conductivity (S cm^{-1})	t_{Li^+}	ESW (V)	Mechanical properties	Thermal properties	Ref
Miscible/ Immiscible Blend	PMMA/ PEO-$LiClO_4$	4.3×10^{-6} (25 °C) 1.3×10^{-5} (60 °C)	–	–	–	–	33
	PEO /PPC-LiTFSI	2.04×10^{-5} (25 °C) 2.82×10^{-5} (60 °C)	0.184	4.9	–	–	35
	PVDF-HFP /PVP-LiTFSI	2.84×10^{-4} (25 °C)	0.45	4.53	–	Stable up to 380 °C	56
	PEO /PVDF-LiTFSI	1.4×10^{-4} (30 °C)	–	–	–	–	57
Block Copolymers	(Polystyrene-b-PEO)-LiTFSI	1.6×10^{-2} (25 °C) 1.8×10^{-1} (65 °C)	0.31	5.1	G modulus of 1 GPa	Stable up to 331 °C	42
	PVBmPEO2000-*b*-PS + $Pyr_{14}TFSI$	0.9×10^{-3} (40 °C)	0.009	–	–	Stable up to 353 °C	39
	PVBmPEO2000-*b*-PS + $Pyr_{O7}TFSI$	0.29×10^{-3} (40 °C)	0.059	–	–	Stable up to 327 °C	39
	P(AA-co-PEGA)-b-PCL-LiTFSI	8.9×10^{-5} (30 °C)	0.12	4.2	–	–	58
	PBnMA–b– (PCL-r-PTMC)-LiTFSI	9.1×10^{-6} (30 °C)	0.64	–	Storage modulus of 0.2 GPa	–	40
Semi-IPN	(ETPTA/PVdF-HFP) + PCE-LiTFSI	4×10^{-3} (25 °C)	–	5	–	–	46
	(PETMP/PAL)+PEGDME-LiTFSI	7.62×10^{-4} (30 °C)	–	5.66	–	–	47
	(PEG/POSS +PPC-LiTFSI	3.3×10^{-5} (40 °C) 6.2×10^{-4} (90 °C)	0.4	–	–	–	48
	PEO-PEGdMA-LiTFSI	$1 \times 10^{-4.04}$ (40 °C) $1 \times 10^{-3.52}$ (60 °C)	–	4.6	Compressive stress of 0.28MPa	–	49
	(PEG/POSS)+ PAN-LiTFSI	1.95×10^{-4} (40 °C) 7.86×10^{-4} (90 °C)	–	5.1	–	–	50
	(EGDMA/VEC)+ PVDF-HFP + EC-LiTFSI	1.03×10^{-3} (25 °C) 3.38×10^{-3} (65 °C)	0.36	4.65	Compression Stress of 1.0 MPa	Stable up to 100 °C	51
Full IPN	(CTA/ PEGDMA)+ PEO + [BMIM][TFSI] -LiTFSI	2.84×10^{-3} (25 °C)	0.43	5.2	Tensile strength of 3.5 MPa	Stable up to 305 °C	43
Grafted/Brush Copolymers	(PtBPMA-g-PEG)+ (PVDF-HFP)-LiTFSI	4.49×10^{-5} (30 °C)	0.6	4.8	Tensile strength of 2.60 MPa	Stable up to 300 °C	30
	PC-g-TEG+ (PVDF-HFP)-LiTFSI	2×10^{-5} (30 °C)	0.67	4.5	Stable up to 1.18 MPa	–	52
	poly(MMA-g-$POEM_5$)- $LiClO_4$	2×10^{-5} (30 °C)	–	–	Tensile strength of 1 MPa	–	55

Abbreviations: ESW, Electrochemical stable window; PMMA, Polymethyl methacrylate; PEO, Polyethylene oxide;$LiClO_4$,Lithium perchlorate; PPC, Polypropylene carbonate; LiTFSI , Lithium bis(trifluoromethanesulfonyl)imide; PVDF-HFP, Polyvinylidene fluoride-co-hexafluoropropylene; PVP, Polyvinylpyrrolidone; PVDF-TrFE, Polyvinylidene fluoride-co-trifluoroethylene ; PC, Propylene carbonate; PVBmPEO,poly(vinyl benzyl methoxy poly(ethylene oxide) ether); PS, Polystyrene ; PAA, Polyacrylic acid; PEGA, Polyethylene glycol; PCL, Poly(**ε**-caprolactone); PbnMA,Polybenzyl methacrylate; PTMC, Polytrimethylene carbonate; ETPTA, Ethoxylated trimethylolpropane triacrylate; PCE, Plasti crystal electrolytes; PETMP, Pentaerythritol tetrakis (3-mercaptopropionate); PAL, hexakis(allyloxy)cyclotriphosphazene; PEGDME,Poly(ethylene glycol) dimethyl ether; PEG, Polyethylene glycol; POSS, polyhedral oligomeric silsesquioxane; PAN, Polyacrylonitrile; EGDMA, Ethylene glycol dimethacrylate; VEC, Vinylethylene carbonate; EC, Ethylene Carbonate; MMA, Methyl methacrylate

coworkers observed two transitions at low salt contents, indicating phase separation, but a single T_g at higher LiTFSI ratios, consistent with a homogeneous amorphous phase and a reduced χ_{eff} as shown in Figure 1E.[29] This evolution correlated with the effective interaction parameter extracted from scattering and thermal analysis, which became negative at elevated salt loading, reflecting salt induced compatibilization.

Ion transport in blends remains strongly coupled to segmental motion. Low T_g polymers such as PEO enable chain relaxation above ambient temperature and support lithium hopping between coordinating sites, whereas high T_g polymers like PVP restrict segmental mobility and suppress conductivity. Salt coordination occurs through polar functional groups, for example ether oxygens in PEO, amide groups in PVP, and carbonate units in PPC. Short chain plasticizers (such as low molecular weight PEO_{400}) lower T_g and create liquid like domains that enhance lithium solvation and ion–dipole interactions. The hydrogen bonded PMAA/PEO complex loaded with $LiClO_4$ illustrates this strategy: miscibility through interpolymer complexation produces a polar, percolated domain that supports lithium conduction, reaching conductivities of order 10^{-6} to 10^{-5} S cm^{-1} between 25 and 60 °C, with further gains upon plasticization with polar carbonate solvents [33].

Miscible blends such as PEO/PMMA suppress crystallinity and form homogeneous amorphous films with a single T_g. Conductivity gains of one to two orders of magnitude over neat PEO at room temperature arise from accelerated segmental relaxation and increased dielectric strength rather than crystallinity reduction alone.[34] Similarly, PEO/PPC blends decrease crystallinity, yield a single T_g , and create a more polar environment that promotes anion dissociation, improving bulk conductivity and interfacial contact at comparable salt contents.[19,35]

In immiscible systems, ion transport occurs through co-continuous amorphous domains rather than a single phase. Here, the efficiency of transport is governed by the percolation threshold, which represents the critical φ required for the conductive phase to form a long range, continuous pathway. This demonstrates that macroscopic performance is a function of phase

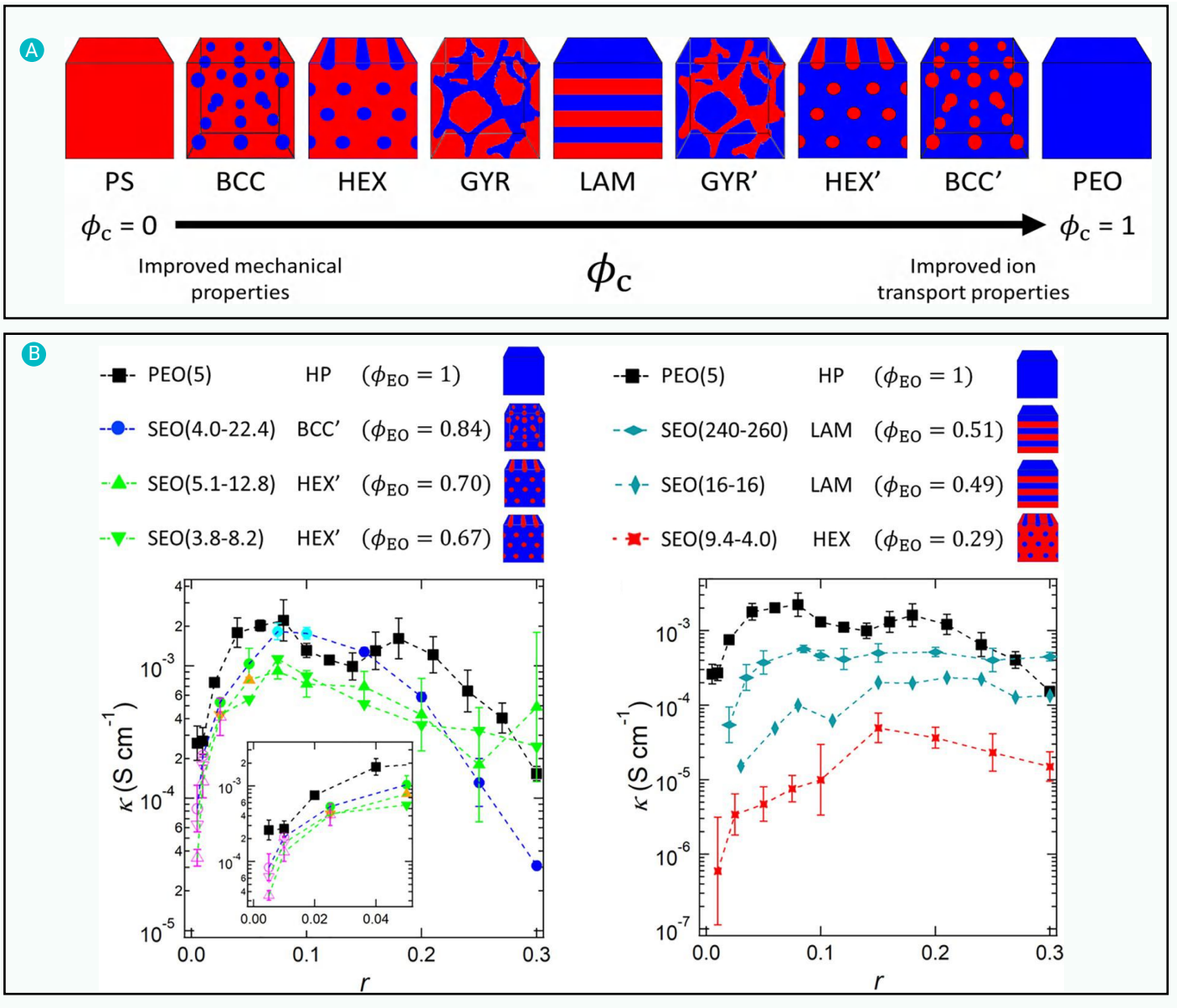

Figure 2. (A) Block copolymer (BCP) morphologies as a function of conducting phase volume fraction, ϕ_c, PS depicted in red and PEO with LiTFSI depicted in blue. (B) Conductivity, κ, of PEO and various SEO electrolytes as a function of r, the molar ratio of lithium ions to ether oxygens for the polymers listed in the figure, where k vs r for PEO and BCP electrolytes with 3d conducting morphologies and k vs r for PEO and BCP electrolytes with 2d and 1d conducting morphologies. Reproduced with permission from Ref.[37]. Copyright © 2020 American Chemical Society.

continuity, phase separation is not inherently limiting provided the φ to exceed the percolation threshold sure a low resistance conducting network.[36]

Collectively, blend based all polymer HSPEs demonstrate that electrolyte performance is governed by phase architecture, where thermodynamic control, domain continuity, dielectric environment, and segmental mobility must be engineered to maximize ion transport while preserving mechanical integrity.

Block copolymers (BCPs). BCP electrolytes use thermodynamically driven microphase separation to spatially decouple ion transport from mechanical reinforcement. In contrast to random blends, where phase morphology is difficult to control, block copolymers self-assemble into well-defined nanostructures such as lamellae, cylinders, spheres, and gyroids (Figure 2A) when the product χN and block volume fractions exceed critical values.[38] In these systems, one block is typically a polar, salt solvating phase (often PEO or related ethers) and the other is a glassy or elastomeric phase that provides mechanical strength and dimensional stability. Microphase separation generates a periodic arrangement of conducting and load bearing domains on the 10–50 nm scale. The morphology and domain spacing are determined by the volume fraction of the conducting phase (φ_c), the total degree of polymerization, and the interaction parameter χ.[39,40] When the conducting block percolates, the ionic phase forms continuous nanochannels that support lithium transport. The nonconducting block forms a continuous matrix that suppresses dendrite growth and maintains separator integrity. Salt ions partition preferentially into the solvating domains, and confinement of PEO within these nanodomains suppresses long range crystallization when domain size falls below the PEO crystallite length scale.

Mechanically robust di-block systems demonstrate this design logic. Bergfelt and coworkers reported Polybenzyl methacrylate -b- poly(ε-caprolactone-r-trimethylene carbonate) (PBnMA–*b*–(PCL-*r*-PTMC)) electrolytes salted with LiTFSI, achieving room temperature conductivities near 10^{-5} S cm^{-1} and a t_{Li^+} of approximately 0.64, while maintaining a storage modulus of about 0.2 GPa.[40] The rigid block limits dendrite penetration, and the soft, carbonate rich block maintains sufficient segmental mobility. He et al. designed difunctional BCPs in which UV cross linkable groups were placed in the rigid block, while pendant PEG side chains in the soft block supplied coordination sites. These membranes reached conductivities above 6×10^{-4} S cm^{-1} at room temperature, with t_{Li^+} around 0.35 and interfacial resistances below 80 Ω cm^2, significantly outperforming linear PEO controls.[41]

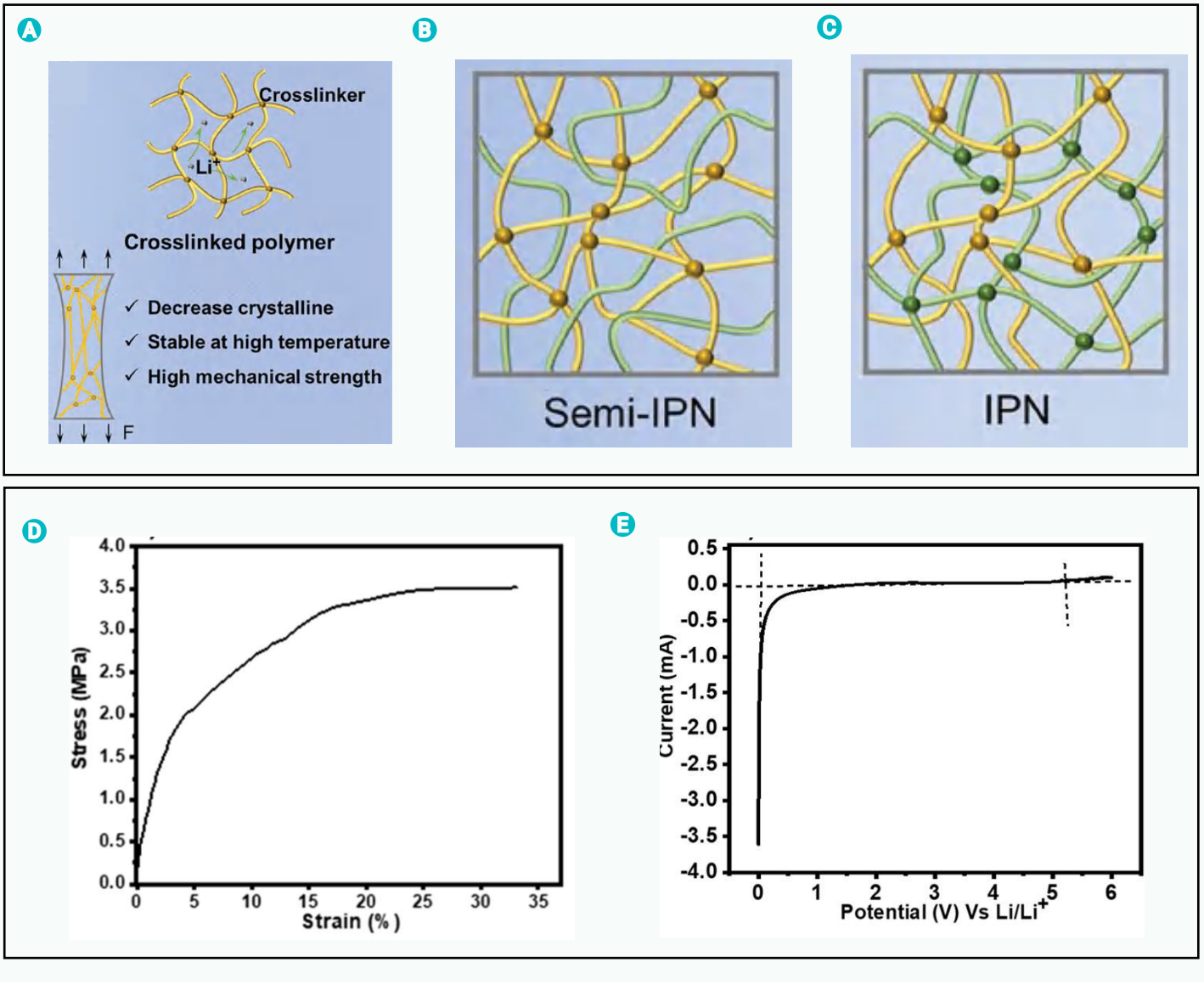

Figure 3. (A) Schematic illustration for ion transport and characteristics of crosslinked polymer. Schematic illustration of the network structure of (B) Semi Interpenetrating Network (Semi IPN) and (C) Interpenetrating Network (IPN). Reproduced with permission from Ref.[21]. Copyright © 2024 Wiley-VCH GmbH. (D) Stress vs strain curve for the IPN electrolyte membrane. (E) LSV curve of Li/IPN membrane/SS cell at scan rate of 0.1 mV s^{-1}.Reproduced with permission from Ref.[43]. Copyright © 2022, American Chemical Society.

Styrenic backbones with PEO side chains extend this approach. Butzelaar et al. synthesized side chain block copolymers with suppressed PEO crystallinity, reporting conductivities near 1.6×10^{-5} S cm^{-1} at 25 °C and 1.8×10^{-4} S cm^{-1} at 65 °C, with oxidative stability enhanced by styrene domains.[42] Incorporation of ionic liquids further boosted conductivity to about 0.18 mS cm^{-1} at 40 °C, while functional ionic liquids improved lithium transference at slightly lower bulk conductivity, illustrating how selective plasticization of the conducting domains tunes both bulk transport and interfacial behavior.[39] This principle translates directly to semi crystalline homopolymer architectures like PVDF, where the host matrix utilizes its natural crystalline amorphous morphology to decouple mechanical stiffness from fast bulk transport, allowing entrapped ionic liquids to lower transport resistance without compromising structural modulus.[28]

The influence of morphology on conduction has been quantified by Galluzzo et al., who related conductivity to the volume fraction of the conducting phase and the connectivity of PEO rich domains.[37] When φ_c is low, conducting domains are isolated and conductivity is poor. As φ_c increases and the conducting phase becomes continuous, conductivity rises, with three-dimensional conducting morphologies outperforming one- and two-dimensional connectivity at equivalent volume fractions (Figure 2B). This morphological hierarchy directly dictates the τ of the ion transport path. While one-dimensional (cylindrical) or two-dimensional (lamellar) morphologies can achieve high conductivity when perfectly aligned, their randomly oriented polycrystalline forms in bulk membranes lead to high effective τ and grain boundary resistance. In contrast, three dimensionally interconnected phases, such as the gyroid morphology, provide a continuous conducting network with a τ factor approaching unity. By minimizing the geometric deviation of the lithium-ion path, these architectures maximize the effective diffusion coefficient and ensure homogeneous current distribution, which is critical for suppressing local field intensification and dendrite nucleation.

Overall, Effective design of BCP electrolyte requires a polar block that forms largely amorphous, continuous ion conducting domains at practical ϕ_c, paired with a mechanically robust block that provides a continuous matrix to suppress dendrites, tolerate stack pressure, and enhance oxidative stability. Morphology should be directed through χ_N and volume fraction control to produce interconnected pathways (e.g., gyroid or cylindrical networks) rather than isolated domains, while cross linkable or high T_g motifs in the rigid block help stabilize the nanostructure during elevated temperatures and electrochemical cycling.

Interpenetrating polymer networks (IPNs). Interpenetrating polymer

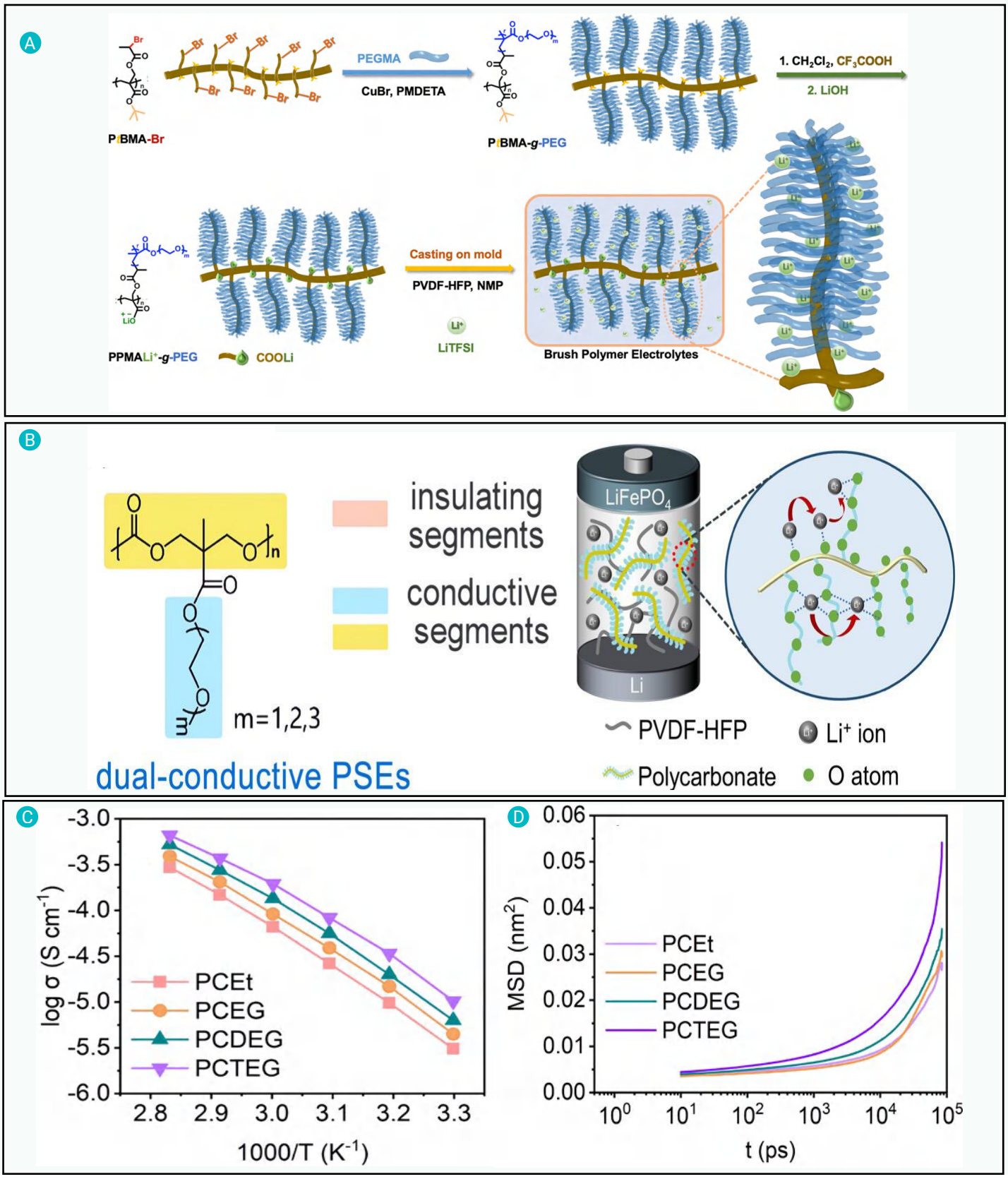

Figure 4. (A) Synthetic route of molecular brush PPMALi-g-PEG. Reproduced with permission from Ref.[30]. Copyright © 2019, American Chemical Society. (B) Brush copolymers with PC backbones and PEO side chains, and both are ion conductive (C) σ of PC/LiTFSI polymer electrolytes as a function of temperature (D) mean squared displacement (MSD) of lithium ions. Reproduced with permission from Ref.[52]. Copyright © 2024, American Chemical Society.

networks are formed when two or more networks are synthesized and crosslinked within each other without covalent bonding between them, allowing decoupled optimization of ion transport and mechanical strength by assigning one network to ion solvation and segmental mobility and the other to rigidity and thermal stability (Figure 3A). Semi IPNs consist of a permanently crosslinked network containing a linear or branched second polymer

(Figure 3B), whereas full IPNs comprise two crosslinked co continuous networks that cannot be separated without bond cleavage (Figure 3C). A central control parameter in IPNs is crosslink density. Classical rubber elasticity relates the shear modulus to the average molecular mass between crosslinks M_c as

$$G = \frac{\rho RT}{M_c},$$

where ρ is network density and R is the gas constant. Increasing crosslink density raises modulus and improves dimensional stability but reduces free volume and segmental mobility, which can suppress σ.[21] Larger M_c values lower T_g and enhance chain motion in amorphous domains. Balancing these effects allows IPNs to reach conductivity modulus windows that are difficult to obtain in single network polymers.

Beyond crosslink density, the performance of IPNs is defined by the interfacial thickness and the degree of molecular interlacing.[44] Unlike immiscible blends where phase boundaries are distinct and can act as barriers to ion transport, the forced compatibility of an IPN creates a broad, diffuse interface at the nanometer scale. This architectural feature maximizes the contact area between the ion conducting and load bearing phases without macroscopic phase separation. Consequently, the percolation of the conductive phase is achieved at the molecular level,[45] ensuring that the lithium ion pathways are intrinsically continuous throughout the rigid scaffold, which effectively lowers the interfacial resistance and stabilizes the electrolyte against salt segregation during high rate cycling.

Semi IPNs suppress crystallinity while preserving chain mobility by embedding a flexible solvating phase within a rigid scaffold. Ha et al. incorporated linear PVDF HFP into a UV cured ethoxylated trimethylolpropane triacrylate (ETPTA) network, forming a deformable electrolyte with two distinct T_g values near −21 °C and 74 °C, confirming retention of a soft conducting phase within a stiff framework.[46] Suk et al. Thiol-ene derived semi IPNs prepared in situ thiol–ene polymerization within PEGDME/LiTFSI similarly reduced crystallinity and generated continuous amorphous pathways that support ion transport and electrochemical stability.[47] Incorporation of linear PPC into a PEG/POSS network altered lithium coordination, weakened excessive lithium PEO interactions, lowered VTF activation energy, and increased t_{Li^+}, with optimal conductivity at moderate PPC content before phase separation emerged.[48]

Embedding PEO within rigid semi IPN matrices also homogenizes morphology. Increasing salt content to an EO:Li ratio of 10:1 eliminated the PEO melting transition and produced a fully amorphous, uniform surface by DSC and AFM, correlating with improved conductivity and more homogeneous lithium deposition through reduced local field intensification.[49] Introducing nitrile containing phases such as PAN enhanced oxidative tolerance and interfacial stability via strong dipolar interactions,[50] while carbonate rich networks based on PVEC and PVDF-HFP improved flexibility and mechanical durability during cycling.[51]

Full IPNs provide greater structural robustness through two covalently interpenetrating networks. A PEO, polyethylene glycol dimethyl acrylate (PEGDMA), cellulose triacetate (CTA) system plasticized with 1-Butyl 3-Methyl Imidazolium Bis-(trifluoromethanesulfonyl) Imide [BMIM][TFSI] yielded highly amorphous membranes with improved thermal stability, tensile strength near 3.5 MPa, elongation around 33% (Figure 3D), and an extended electrochemical window (Figure 3E) while maintaining effective ion transport.[43]

Overall, IPNs decouple conduction from mechanical function through architectural control: semi IPNs prioritize segmental mobility within a supportive framework, whereas full IPNs maximize dimensional stability, with performance governed by crosslink density, phase continuity, and functional group selection that enhances polarity or oxidative stability without inducing macro phase separation.

Graft Copolymers. Graft copolymer electrolytes decouple ion transport from mechanical response by attaching solvating side chains to a mechanically robust backbone. Dense grafting suppresses crystallization, increases amorphous content, and concentrates coordination sites without substantially reducing backbone T_g, while backbone chemistry, side chain length, and graft density govern segmental relaxation, salt binding, and the rigidity mobility balance.[53] Here, the primary topological parameters are the graft density and the pendant chain length, which collectively define the characteristic domain spacing. When integrated with block scaffolds, mixed graft block copolymers self-assemble into ion rich domains within a load bearing matrix, where microphase separation confines amorphous channels and preserves mechanical integrity, a topology well suited for thin membranes requiring continuous conduction paths.[54]

Unlike linear chains, the dense attachment of solvating grafts creates a bottlebrush effect that forces the backbone into an extended conformation. This suppresses the formation of large-scale crystalline regions by reducing the available volume for chain folding. Consequently, the ion transport performance is governed by the local coordination density, the proximity of side chains enables a hopping mechanism where the energy barrier for ion transport is decoupled from the long range relaxation of the polymer backbone, effectively increasing the t_{Li^+} (Figure 4A).[30] Blending with PVDF HFP yields free standing films with tensile strength around 2.6 MPa and stability up to about 4.8 V, demonstrating practical viability. Structure property studies show that longer branched chains enhance conductivity, with Poly oligo(oxyethylene) methacrylate ($POEM_9$) based systems exhibiting roughly tenfold higher conductivity than $POEM_5$ across [Li]/[EO] ratios, whereas shorter spacing and higher chloromethylstyrene (CMS) content improve tensile strength, all systems maintain strengths above 1 MPa, underscoring the tradeoff between mobility and modulus.[55]

Grafted polycarbonates bearing ethylene oxide side chains further demonstrate that both backbone and side chains can participate in lithium transport (Figure 4B-D).[52] Increasing ethylene oxide units lowers T_g and enhances segmental mobility, raising conductivity in agreement with molecular dynamics predictions of lithium diffusion trends. At 30 wt.% LiTFSI, optimized compositions deliver conductivities around 1×10^{-5} S cm^{-1} at 30 °C, t_{Li^+} near 0.67, and oxidative stability to about 4.5 V.[52] Blending with PVDF- HFP affords membranes with tensile strength near 1.2 MPa and stable lithium symmetric cycling over 1600 h, confirming that conductive backbones can raise transference number without sacrificing mechanical strength.[52]

Transport in graft systems is further shaped by mesoscale organization and processing, which control side chain packing and defect density. Scattering and dielectric analyses indicate that ion motion often involves hopping across nanophase boundaries at high salt loading, while dense grafting distributes stress, limits creep under stack pressure and maintains interfacial contact with lithium metal.

Overall, graft and brush architectures provide architectural control over nanoscale solvation and macroscopic mechanics, where continuous amorphous pathways, mechanically stable backbones, organized conducting domains, and defect minimized processing collectively determine electrolyte performance.

Network engineered polymer architectures (polymer-inorganic HSPEs)

Polymer-inorganic HSPEs embed rigid ceramic phases such as oxides, sulfides, nanosheets or porous frameworks within polymer matrices to enhance ion transport, mechanical strength, thermal and electrochemical stability. The inorganic phase may serve as passive reinforcement that suppresses crystallinity and modulates dielectric properties or as an active lithium conductor, while geometric control from dispersed particles to continuous three-dimensional scaffolds decouple stiffness from segmental mobility and creates preferential transport pathways. In these hybrid systems, the macroscopic performance is governed by three critical architectural parameters:

- Percolation threshold of the inorganic phase
- τ of the resulting ion pathways
- Characteristic Debye length(λ_D) of the space charge regions at the polymer-ceramic interface.

Conductivity depends on filler connectivity: below percolation, interfacial regions dominate transport, near or above percolation, one- or two-dimensional networks reduce τ and fully infiltrated three-dimensional frameworks enable bicontinuous conduction through ceramic, polymer and interfaces. Interfacial engineering through surface functionalization, grafting, or core shell design improves dispersion and ion transfer while limiting agglomeration and space charge effects. Despite scalable processing routes such as

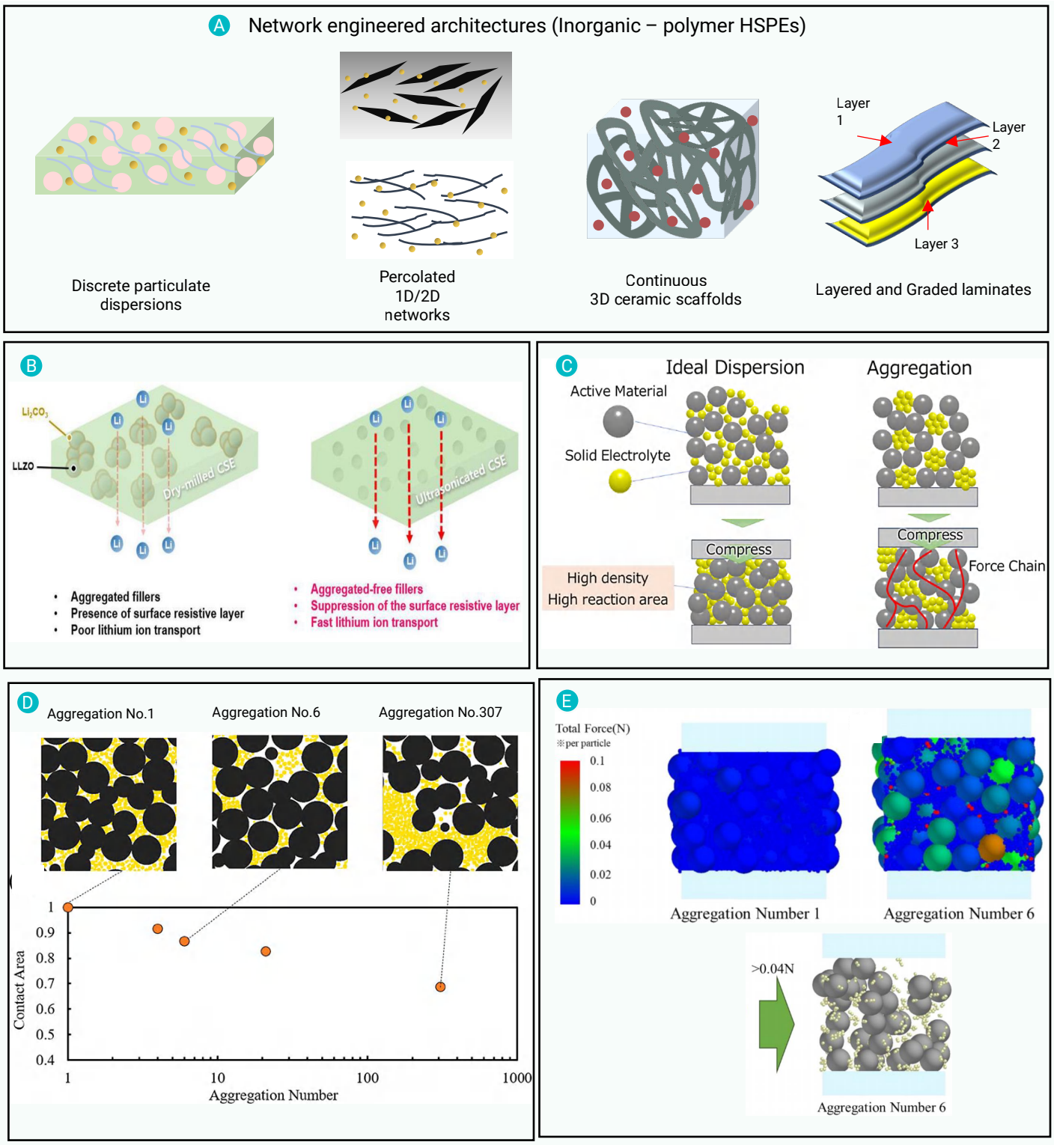

Figure 5. (A) Network engineered polymer architectures. (B) Schematic of HSPE with aggregated particles and aggregated-free particles. Reproduced with permission from Ref.[59]. Copyright © 2023, American Chemical Society. (C) Schematic of ideal and aggregation mechanism during compression. (D) Cross sectional images of the electrode for aggregation numbers of 1, 6, and 307 and the Relationship between reaction area and aggregation number. The black particles represent the active material particles, and the yellow particles represent single particle of the solid electrolyte. Reaction area was normalized to the ideal dispersed state as 1. (E) Stress distributions for aggregation numbers 1 and 6, respectively, represented by a color map of the total force on each particle and only the particles with an aggregation number of 6 that were subjected to a force greater than 0.04 N. Reproduced with permission from Ref.[60]. Copyright © 2025, The Author(s). Published by ECSJ.

blending, in situ polymerization, sol gel formation, templating and hot pressing, key challenges remain in achieving high room temperature conductivity with adequate modulus, low interfacial resistance, cycling stability, and wide oxidative tolerance, thus these systems are best classified by filler network architecture into discrete, percolated, continuous scaffold or layered configurations as given in Figure 5A (Table 2).

Discrete Particulate Dispersions. In discrete particulate dispersion (DPD) solid polymer electrolytes, a continuous polymer matrix such as PEO, PMMA, PVDF, or PAN contains non percolating inorganic particles that modify segmental dynamics, salt dissociation, and interfacial transport without forming a continuous ceramic network (Figure 5B). Beyond traditional inorganic fillers, recent advances include the use of functional microcapsules,

Table 2. Summary of network engineered polymer architectures: polymer-inorganic HSPEs.

Filler-network architecture	Electrolyte composition	Ionic conductivity (S cm^{-1})	t_{Li^+}	ESW (V)	Mechanical strength	Thermal stability	Ref.
Discrete Particulate Dispersion	PEO - $Li_{6.4}La_3Zr_{1.4}Ta_{0.6}O_{12}$ - LiTFSI	4.4×10^{-4} (70 °C)	0.379	–	–	–	59
	PEO - $Li_{6.4}La_3Zr_{1.4}Ta_{0.6}O_{12}$ - LiTFSI	2.31×10^{-4} (30 °C)	0.39	4.8	–	–	62
	PEO- silane-LiTFSI	7.67×10^{-5} (25 °C)	0.34	4.84	–	–	63
	PPC- MSN -LiTFSI	8.48×10^{-4} (60 °C)	0.86	4.8	Tensile strength of 500 KPa	Stable upto 180 °C	91
	PEO- $BaTiO_3$-LiTFSI	2.2×10^{-5} (25 °C)	0.197		–	–	92
	PEO + CSBO -SiO_2- LiTFSI	7.86×10^{-6} (20 °C) 3.98×10^{-4} (80 °C)	-	4.84	–	Stable upto 450 °C	93
Percolated 1D/2D Networks	PAN-$Li_7La_3Zr_2O_{12}$ - $LiClO_4$	1.3×10^{-4} (20 °C)	0.3	–	–	–	94
	PVDF-HFP-$Li_7La_3Zr_2O_{12}$- LiTFSI	9.5×10^{-4} (20 °C)	–	5.2	Tensile stress of 5.3 MPa	Stable up to 350 °C	95
	PAN- $Li_{0.33}La_{0.557}TiO_3$- $LiClO_4$	2.4×10^{-4} (25 °C)	–	–	–	–	96
	PAN- well aligned $Li_{0.33}La_{0.557}TiO_3$- $LiClO_4$	6.05×10^{-5} (30 °C)	–	–	–	–	97
	PEO-vertically aligned $Li_{1+x}Al_xTi_{2-x}(PO_4)_3$- LiTFSI	0.52×10^{-4} (25 °C)	–	–	–	–	98
	PEO-$Li_7La_3Zr_2O_{12}$-LiTFSI	5.44×10^{-5}	0.72	5.1	Maximum stress of 5.28 Mpa	Stable upto 368 °C	99
	PEO-LiTFSI-vertical $Li_7La_3Zr_2O_{12}$ sheet arrays/PAN-LiTFSI	2.6×10^{-4} (25 °C)	0.83	5.1	–	–	100
	PVDF-$Li_7La_3Zr_2O_{12}$- $LiClO_4$	1.16×10^{-4} (30 °C)	-	5	Stress of 1.2-1.8 Mpa	Stable upto 150 °C	101
	PVDF- VNT-$LiClO_4$	2.2×10^{-3}(25 °C) 1×10^{-2} (60 °C)	0.58	5.2	Young module of 18 Gpa	–	102
	PEO-$Mg_2B_2O_5$-LiTFSI	1.53×10^{-6}(40 °C)	0.44	4.75	Maximum stress of 2.29 MPa (5% $Mg_2B_2O5_5$)	–	68
	PEO-MnO_2-LiTFSI	1.95×10^{-5} (30 °C)	0.378	4.5	Tensile strength of 0.56 MPa	–	103
	PEO-CeO_2-LiTFSI	1.1×10^{-3} (60 °C)	–	5.1	Young modulus of 33 MPa	–	104
	PEO-$Li_7La_3Zr_2O_{12}$- $LiClO_4$	3.6×10^{-4} (25 °C)	–	–	–	–	69
	PEO-$Li_7La_3Zr_2O_{12}$ -LiTFSI	1.3×10^{-3} (30 °C)	0.91	–	–	–	105
	PEO- $Li_{6.25}La_3Zr_2AlO_{0.25}O_{12}$ -LiTFSI	4.3×10^{-5} (25 °C)	–	5.3	–	–	106
Continous 3D ceramic scaffolds	PEO- $Li_{0.33}La_{0.557}TiO_3$-LiTFSI	1.5×10^{-4} (30 °C)	–	4.5	–	Stable upto 550 °C	107
	Epoxy-gyroid $Li_{1.5}Al_{0.5}Ge_{1.5}(PO_4)_3$	1.6×10^{-4} (25 °C)	–	–	Elastic modulus of 44 GPa	–	108
	PEO-$Li_7La_3Zr_2O_{12}$-LiTFSI	8.89×10^{-5} (30 °C)	0.49	5.1	Young modulus of 7.24 MPa	Stable upto 320 °C	109
	PEO-$Li_{1+x}Al_xTi_{1.7}(PO_4)_3$-LiTFSI	7.47×10^{-4} (60 °C)	–	5.1	–	Stable upto 330 °C	110
	PCL-$Li_7La_3Zr_2O_{12}$-LiTFSI	0.9×10^{-4} (25 °C)	0.54	5.2	–	–	111
	PEO-$Li_7La_3Zr_2O_{12}$-LiTFSI	8.5×10^{-5} (25 °C)	–	5	–	Stable upto 350 °C	112
Layered or Graded laminates	(PAN-$Li_{1+x}Al_xTi_{2-x}(PO_4)_3$-LiTFSI) + (PEO-SN-LiTFSI)	1.31×10^{-4} (25 °C)	–	5	–	–	82
	(PEO-PEGDME-LiTFSI)-$Li_{1.5}Al_{0.5}Ge_{1.5}(PO_4)_3$	1.25×10^{-4} (25 °C)	–	–	Flexural modulus of 7.8 GPa	–	83
	UV cured PEA network (with LiTFSI, DOL/DME)- $Li_{1.5}Al_{0.5}Ge_{1.5}(PO_4)_3$	7.4×10^{-4} (25 °C)	–	–	Flexural modulus of 7.2 GPa	–	83
	Epoxy-PC-$LiClO_4$-$Li_{1.5}Al_{0.5}Ge_{1.5}(PO_4)_3$	8.4×10^{-4}	–	–	Flexural modulus of 4.5 GPa	–	83

such as polyurea-formaldehyde (PUF) shelled particles. These not only provide structural pathways but act as localized reservoirs for additives like

Table 2. *(Continued)*

Filler-network architecture	Electrolyte composition	Ionic conductivity (S cm^{-1})	t_{Li^+}	ESW (V)	Mechanical strength	Thermal stability	Ref.
	(PVDF-Pyr_{14}TFSI-LLZTO-LiTFSI) + (PAN-LiTFSI)	1.5×10^{-4} (25 °C)	0.72	5	–	–	85
	(15% $Li_{0.33}La_{0.557}TiO_3$-PVDF/$LiClO_4$) + (75% $Li_{0.33}La_{0.557}TiO_3$ -PVDF/$LiClO_4$) + (15% $Li_{0.33}La_{0.557}TiO_3$-PVDF/$LiClO_4$) sandwich structure	4.7×10^{-4} (25 °C)	–	5	Tensile strength of 7.2MPa Young module of 57.1 MPa	Stable upto 390 °C	86
	(PVDF-b-PTFE)- $Li_7La_3Zr_2O_{12}$- $LiN(SO_2CF_3)_2$- $Li_{0.33}La_{0.557}TiO_3$	1.38×10^{-4} (25 °C)	0.58	5.3	Tensile strength of 19 MPa	–	113

Abbreviations: PPC, Poly(propylene) carbonate; MSN, Mesoporous silica nano particles; CSBO, Carbonated soybean oil; VNT, V_2O_5 nanotubes; PEA, Poly(ether-acrylate)

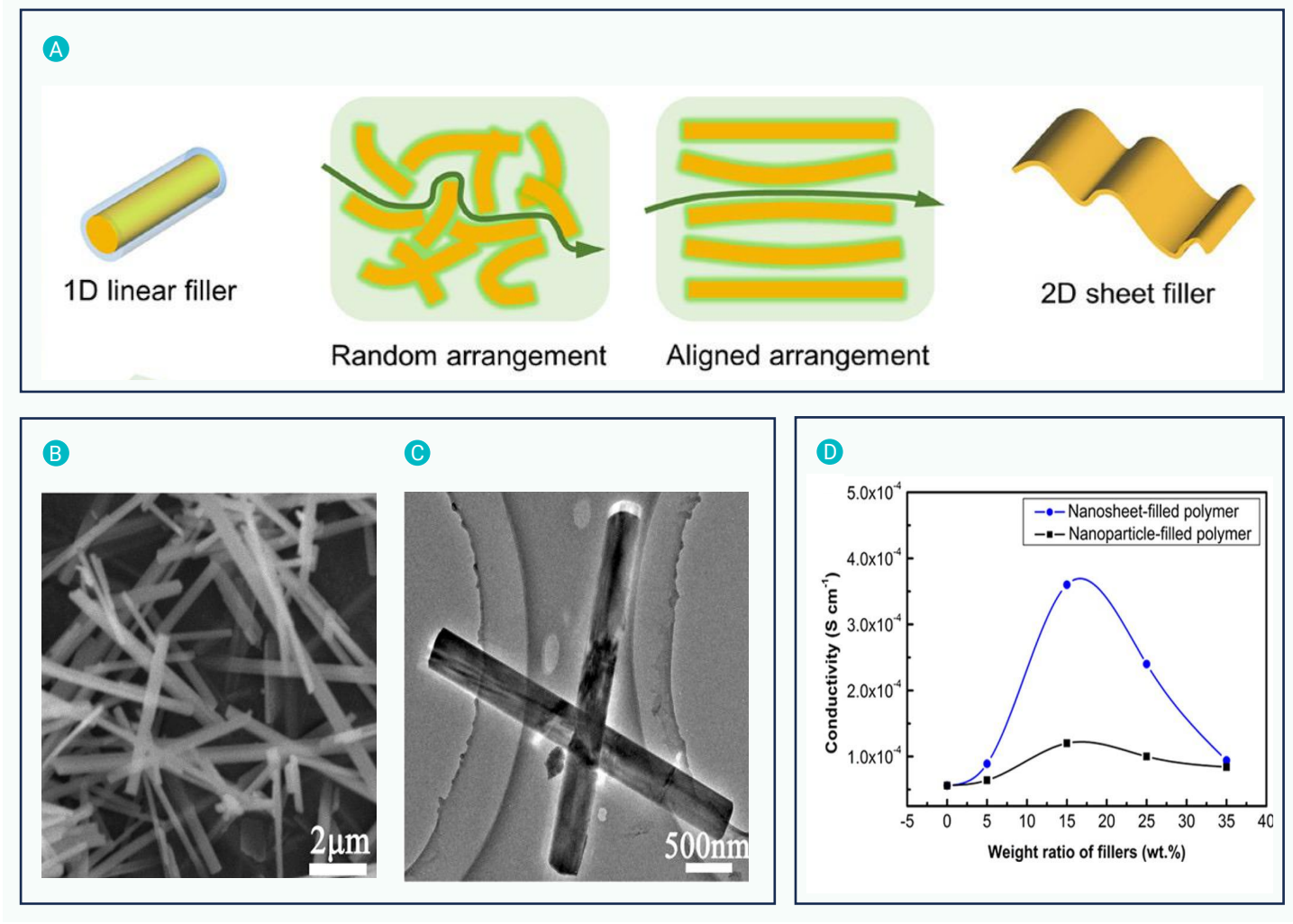

Figure 6. (A) Schematic diagram of the transportation path of Li ions in the PEO based composite polymer electrolyte with 1D, 2D filler morphologies. Reproduced with permission from Ref.[67]. Copyright © 2021, American Chemical Society. Characterization of the $Mg_2B_2O_5$ nanowires (B) SEM image and (C) TEM image. Reproduced with permission from Ref.[68]. Copyright © 2018, American Chemical Society. (D) Conductivity comparison of the composite electrolytes filled with garnet nanosheets and nanoparticles. Reproduced with permission from Ref.[69]. Copyright © 2019, American Chemical Society.

flame retardants (e.g., triphenyl phosphate).[61] Lithium transport arises from solvated polymer segments, ionically active interphases created by Lewis acid base interactions at particle surfaces, and possible surface hopping along high dielectric skins, while the dispersed phase increases stiffness and mitigates concentration polarization.[22] For instance, the encapsulation of flame retardants within a PUF shell has been shown to provide additional Li^+ hopping sites while simultaneously disrupting PEO chain alignment. This structural disruption increases the amorphous fraction of the polymer, facilitating a significant boost in σ.[61]

Conductivity and lithium transference enhancements depend on microstructural control including particle size, aspect ratio, surface chemistry, polymer filler affinity, and processing route, which govern aggregation, interparticle spacing, and interphase thickness; filler contents are typically below about 10 wt% to avoid percolation. In this regime, the architecture is defined

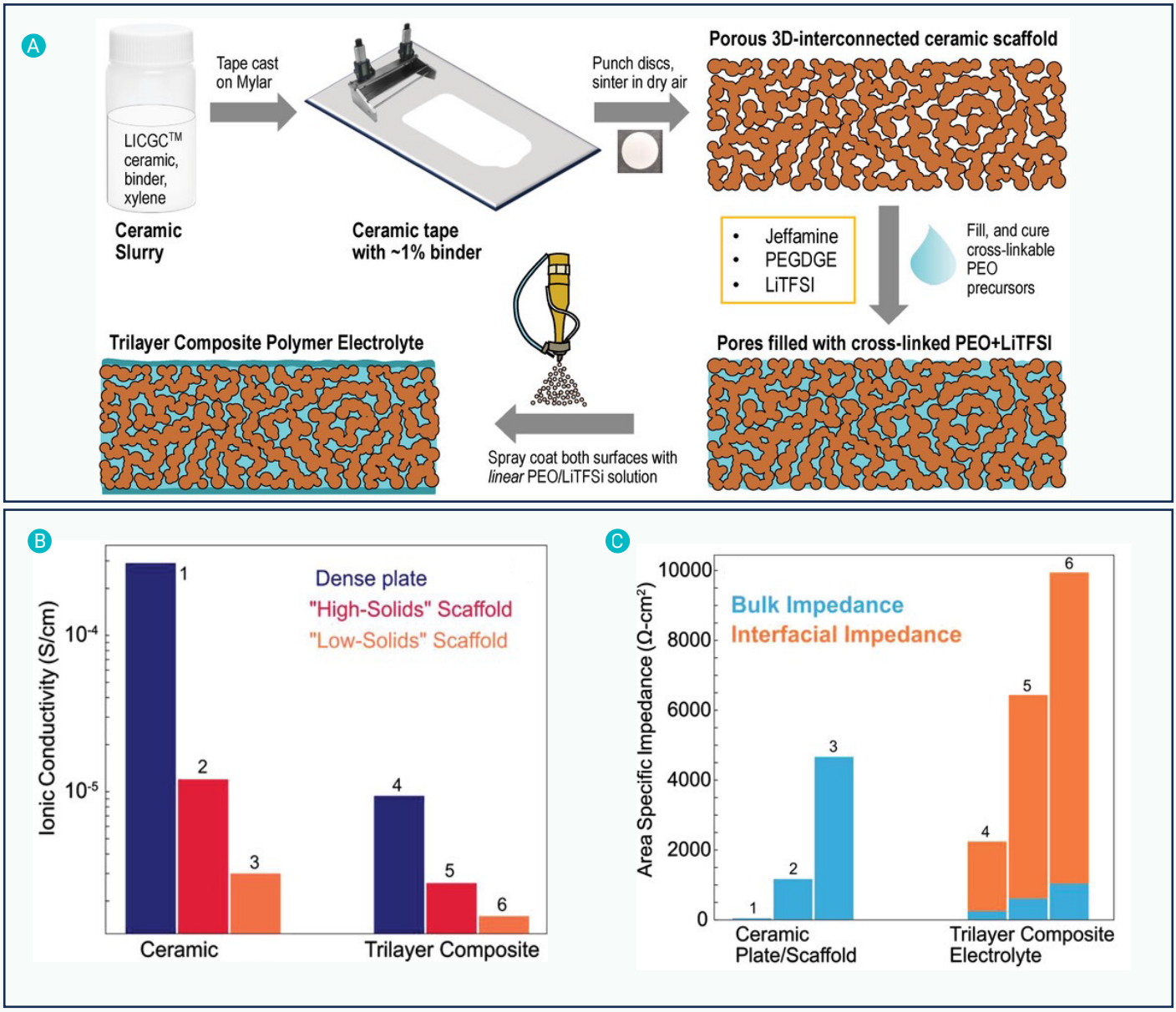

Figure 7. (A) Schematic of Tri layer HSPE with porous LICGC ($Li_{1+x+y}Al_xTi_{2-x}Si_yP_{3-y}O_{12}$) scaffold (B) Bar chart comparing the RT ionic conductivities of the three types of bare ceramic scaffolds (dense ceramic, "high-solids" scaffold, and "low-solids" scaffold) with 0%, 48%, and 52% porosity, respectively, and their corresponding Trilayer HSPEs (C) Bar chart comparing the area specific bulk and interfacial impedance at RT of the six samples (numbered 1–6). Reproduced with permission from Ref. [74]. Copyright © 2023 Wiley-VCH GmbH.

by the interphase volume, the enhancement in σ is proportional to the fraction of polymer chains residing within the λ_D of the filler surface, where Lewis acid-base interactions promote salt dissociation and increase the local concentration of mobile Li^+ ions.[27,59]

Oxides such as SiO_2, Al_2O_3, TiO_2, nitrides such as AlN, sulfides such as Li_2S-P_2S_5, and garnets such as LLZO differ in dielectric constant and surface functionality, enabling hydrogen bonding, tailored interfacial compatibility, enhanced salt dissociation, and reduced agglomeration when properly dispersed at the nanoscale.[62,63,64] Particle scale mechanics during mixing and calendaring further determine coordination number, packing density, and void structure, as shown by discrete element simulations that guide pressure, size distribution, and binder selection to produce dense crack free films with reproducible pathways (Figure 5C).[60] Interfacial engineering can partially decouple lithium transport from bulk segmental relaxation, allowing conductivity retention even as modulus increases if surface chemistry promotes interphase mobility and suppresses anion motion.[65]

A notable advancement in this architecture involves in situ molecular engineering to overcome the characteristic high interfacial resistance of ceramic fillers. For instance, recent work demonstrates the use of the Li_2CO_3 passivation layer on garnet type LLZTO particles as an initiator for the ring opening polymerization of bis(fluoroethyl) carbonate.[66] This process creates fluorine rich oligomers directly on the particle surface, which not only facilitates rapid Li^+ transport through enhanced binding energy but also fosters the formation of a stable, LiF rich solid electrolyte interphase (SEI). Such strategies exemplify how the precise architecture of the particle-polymer interface can simultaneously optimize σ and electrochemical stability in hybrid systems.

Thus, optimal DPD design requires aggregate free dispersions below percolation, surface functionalization that balances cation coordination and anion trapping, controlled processing to minimize voids, and holistic evaluation of conductivity, t_{Li^+}, electrochemical stability, lithium deposition morphology, and mechanical durability (Figure 5D&E).[59-60,62,65] Despite scalability, DPD systems lack continuous fast ion channels, motivating development of partially percolated networks that combine interfacial benefits with extended ceramic conduction pathways.

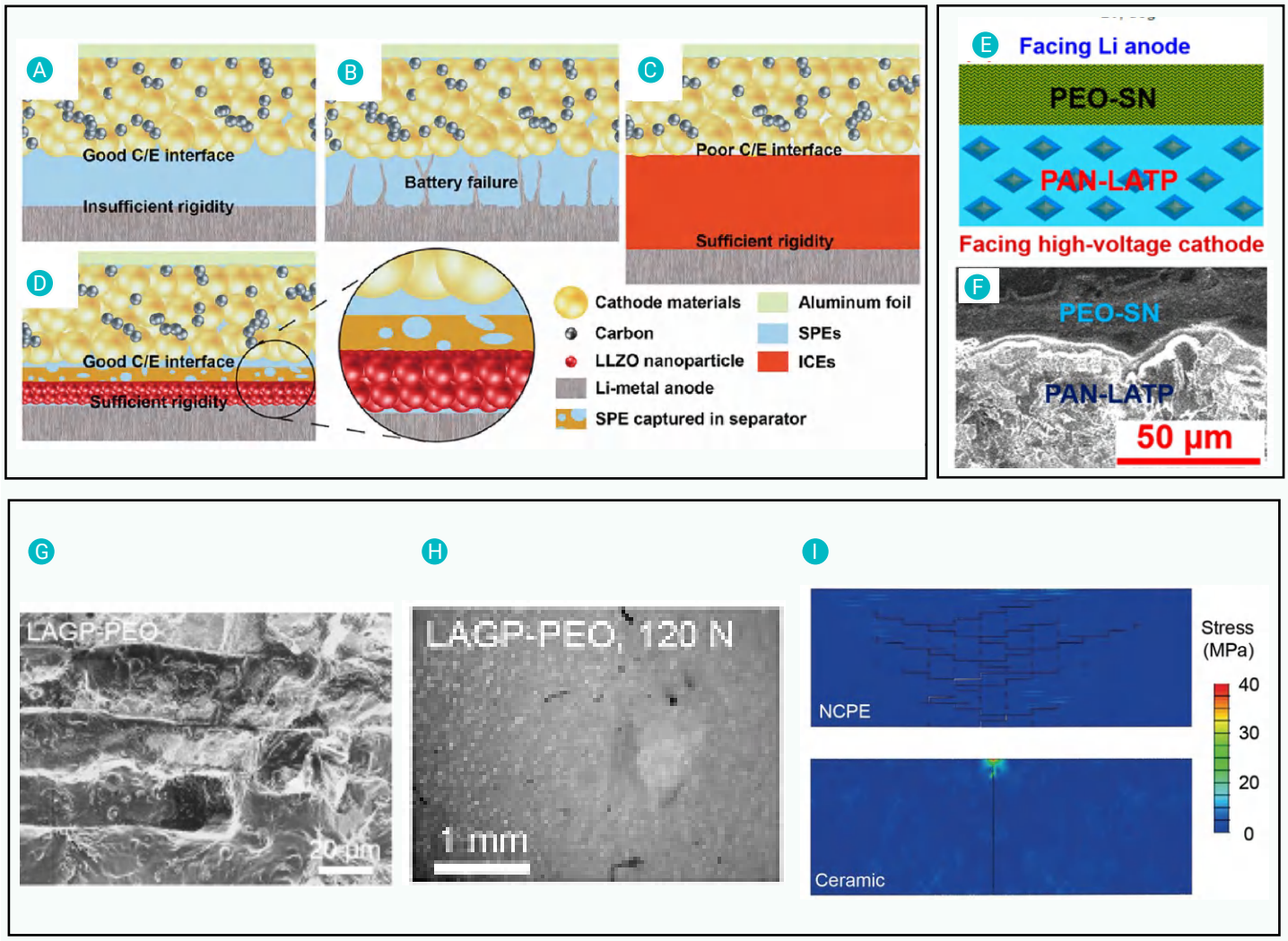

Figure 8. Schematic of solid-state Li battery with ((A) and (B)) conventional SPEs, (C) Inorganic composite electrolyte (ICE) and (D) Multi-layered HSPE. Reproduced with permission from Ref.[81]. Copyright © 2018, American Chemical Society. (E) The PEO-SN / PAN-LATP HSPE(I)Schematic of the laminated dual polymer/polymer-ceramic HSPEs. (F) Cross section SEM image of the PEO-SN-LiTFSI/PAN-LATP-LiTFSI HSPE. Reproduced with permission from Ref.[82]. Copyright © 2020, American Chemical Society. The nacre like LAGP–PEO HSPE (G) Cross sectional SEM images of Hot pressed LAGP–PEO HSPE film showing the staggered microstructure (H) Vickers indentation of nacre like LAGP–PEO HSPE film using loads of 120 N (I) Nonlinear finite element simulations of tortuous crack propagation through interfacial polymer failure in an HSPE film and a straight crack in a pure ceramic film under the same force. Reproduced with permission from Ref.[83]. Copyright © 2019, WILEY-VCH Verlag GmbH & Co. KGaA, Weinheim.

Percolated 1D/2D networks. Percolated 1D/2D HSPEs exploit the low percolation thresholds of high aspect ratio fillers to form continuous inorganic networks within polymers (Figure 6A), unlike discrete dispersions that remain below geometric connectivity. Because critical loading scales inversely with aspect ratio, modest fractions of nanowires, nanotubes (Figure 6B&C), or nanosheets can generate interconnected, high dielectric or intrinsically lithium conductive scaffolds.[70,24,25] The unifying principle here is the inverse relationship between the filler aspect ratio and the percolation threshold. By utilizing 1D nanowires or 2D nanosheets, a continuous inorganic highway is established at significantly lower volume fractions than spherical particles, effectively reducing the macroscopic τ while preserving the polymer like flexibility of the bulk membrane. These architectures partially decouple lithium mobility from polymer segmental relaxation: interfacial regions with altered solvation form quasi continuous conduction channels that sustain current even when the matrix is stiffened, particularly when electronically insulating, ionically cooperative oxides such as LLZO or LLTO are surface cleaned, chemically matched, and functionalized to reduce impedance and suppress voids.[71,25]

One dimensional networks achieve connectivity at very low volume fractions and redistribute interfacial stresses, improving critical current density if rod junction resistance and wetting are controlled,[70,24,25] though excessive connectivity can induce brittleness or anisotropy.[24] Two dimensional nanosheets maximize polymer filler contact, disrupt crystallinity, and create extended space charge regions with low τ transport (Figure 6D), provided platelet junction resistance and electronic leakage are avoided.[67,25] Hybrid rod platelet assemblies further lower percolation thresholds, increase junction redundancy, and enhance isotropy and damage tolerance under compression.[72,73] Ultimately, templating, alignment, solvent selection, calendering, and hot pressing determine network continuity and interfacial wetting, defining a processing window where junction formation exceeds breakage and a large polymer fraction resides within a Debye length of oxide surfaces.[24,25] Key risks include unintended electronic percolation, brittle fracture, interfacial impedance from poor wetting or contaminants, and anisotropic transport from over alignment.[24,70] When electronically insulating oxides, surface functionalization, hybrid one plus two dimensional topologies, and controlled densification are integrated, percolated networks provide a versatile route to transcend the conventional conductivity modulus trade off while preserving interfacial stability and mechanical durability in lithium metal cells.[70,67,25]

Continuous 3D ceramic scaffolds. Continuous 3D ceramic polymer hybrids employ a pre architected, percolating ceramic scaffold (e.g., garnet) that is conformally infiltrated with a polymer - salt phase, guaranteeing through thickness ionic continuity independent of polymer percolation and mitigating the conductivity modulus tradeoff typical of neat SPEs. Long range transport proceeds either through interphase dominated conduction within

thin polymer sheaths wetting ceramic struts (Figure 7A) or via a dual path mechanism in which the Li^+ conductive , electronically insulating ceramic backbone provides a parallel channel, the relative contributions are governed by scaffold τ, pore geometry, nodal coordination, intergranular resistance, and polymer overlayer thickness/chemistry.[74,75] Quantitatively, the 3D scaffold architecture fixes the τ of the fast ion pathway to a near constant value regardless of the polymer's state. This allows for a direct correlation between the scaffold's nodal coordination (connectivity) and the electrolyte's area specific resistance (R_{ASR}), providing a theoretical upper bound for conductivity that is limited only by the grain-boundary resistance of the ceramic struts.

Unlike traditional composite electrolytes that suffer from filler agglomeration at high concentrations, the implementation of a 3D consecutive skeleton allows the inorganic phase to exceed 60 wt% while maintaining structural flexibility and an intact membrane morphology.[76] This architectural design induces multiple synergistic transport pathways, the consecutive ceramic skeleton provides long range continuity, while its large surface area promotes the amorphization of the polymer matrix. Furthermore, the continuous inorganic framework acts as a macroscopic site for anion immobilization, subtly inducing an anion adsorbed interface that serves as a rapid ion immigration channel. By moving from isolated particles to a pre-constructed 3D scaffold, the electrolyte effectively eliminates high interfacial resistance and high concentration polarization, achieving superior σ and a significantly elevated cation transference number.

Architecture property decoupling shows that excessively thick or poorly wetted polymer coatings become the dominant series resistance even at similar porosity, as pore size distribution and node density determine how much polymer resides within a Debye length of oxide surfaces, thereby tuning t_{Li^+}, σ (Figure 7B) and R_{ASR} under pressure (Figure 7C).[74] Thus, optimal performance requires minimizing parasitic "excess surface polymer layers" while ensuring full impregnation and crack free films, alongside low grain boundary resistance within the ceramic backbone bottlenecks.[74,75]

Topological control such as vertically aligned garnet frameworks reduces τ and junction density across thickness, shortens ion pathways, suppresses low frequency polarization, and increases critical current density in Li/Li symmetric cells.[77] Processing kinetics further define functionality: high temperature ultrafast sintering (HTUS) densifies struts and lowers grain boundary resistance without collapsing porosity, whereas over or under sintering compromises impregnation or junction integrity, eroding the benefit of continuity.[75,78] Dimensional scaling to thin (~20 μm), wrapped, and infiltrated 3D ceramics shortens diffusion lengths and enhances interfacial contact, improving Li metal compatibility when surfaces are clean and lithophilic,[79] and the concept extends to lithium - air systems where embedded garnet networks stabilize voltage and reduce overpotential by mitigating polarization gradients deformation.[80]

Collectively, these studies establish a design rule: a low τ, low resistance ceramic skeleton paired with a nanometric, compositionally tuned polymer sheath that preserves interfacial mobility, immobilizes anions, and ensures complete wetting defines a quantitative benchmark via τ, R_{ASR}, t_{Li^+}, and critical current density against which particle based and near percolated architectures can be compared under realistic thickness, stack pressure, and cathode loading constraints.[77,78,79]

Layered or Graded laminates. Layered (multilayer) and graded laminate HSPEs intentionally decouple ion transport, interfacial stability, and mechanical load transfer along the thickness direction by stacking compositionally or morphologically distinct sublayers with strong adhesion (Figure 8A-D), enabling a cathode facing layer optimized for oxidative stability and CEI chemistry, an anode facing layer tailored for lithophilic, high modulus, and anion regulation, and an intermediate core that sustains bulk ionic throughput and structural continuity which is an approach that overcomes the averaged tradeoffs of single phase composites and enables simultaneous gains in conductivity, t_{Li^+}, and critical current density while suppressing parasitic reactions at both electrodes. From an architectural standpoint, laminates introduce anisotropic τ, the structure is designed to have a low through plane τ for rapid ion flux between electrodes, while the layered interfaces provide high lateral resistance to dendrite penetration. This gradient in both chemistry and topology allows for the independent optimization of interfacial energy at the anode and oxidative stability at the cathode.[84,82,83,85]

Dual polymer laminates and polymer/polymer–ceramic hybrids (Figure 8E&F) exemplify this division of labor: oxidation resistant cathode polymers are paired with ceramic rich sublayers that reduce through plane τ and raise modulus, and terminated with soft, lithophilic anode polymers to homogenize Li plating and reduce interfacial impedance where interface targeted gradients in salt content, polymer polarity, and filler fraction stabilize both Li/electrolyte and high voltage cathode interfaces without sacrificing areal power , leveraging controlled space charge and solvation environments at each boundary while preserving continuous ion pathways across internal junctions that require interdiffusion or chemical compatibility to avoid delamination and series resistance.[82,85]

Bioinspired nacre like "brick and mortar" laminates (Figure 8G) extend this concept by embedding aligned, high aspect ratio inorganic platelets within a polymer "mortar," promoting crack deflection and bridging to raise modulus and fracture energy at modest filler loadings (Figure 8H&I) while maintaining polymer mediated Li^+ conduction along interplatelet galleries, platelet size distribution, surface chemistry, orientation (predominantly in plane), and polymer viscosity during layup govern gallery thickness, wetting, and adhesion, and when Li^+ conductive ceramics are selectively incorporated, partial dual path transport improves the conductivity modulus balance at fixed thickness.[83]

Sandwiched and ultrathin (<25–50 μm) multilayer membranes confining ceramic rich or nanofiber reinforced cores between electrode optimized skins minimize R_{ASR} without forfeiting mechanical robustness, provided internal interfaces are ionically transparent and mechanically locked, symmetric Li cells show suppressed low frequency polarization and extended short circuit times as layer thickness and chemistry are tuned , and electro spun lithiated nanofiber interleaves establish "ion highways" across internal boundaries while improving peel strength and shear resistance.[86,87]

Beyond conventional separators, laminate principles extend to multifunctional structural energy composites (e.g., fiber metal and carbon fiber laminates), where electrolyte interleaves must wet adjacent plies, prevent voids, and maintain ionic continuity under compression and cyclic shear, with placement, thickness, and modulus gradients governing both impedance and structural damping.[88,89] Processing strategies including sequential casting, vacuum-assisted layup, hot pressing, and layer by layer assembly permit independent optimization of salt content, molecular weight, and filler loading in each sublayer prior to consolidation, overcoming single bath composite limitations, achieving low internal junction resistance requires miscible or interpenetrating polymer pairs, controlled interdiffusion during curing, and, where necessary, coupling agents or surface activation to ensure entanglement and suppress delamination.[82,83,86]

Framed as a design architecture, layered and graded laminates provide a thickness resolved platform in which interfacial chemistry, ionic transport topology, and mechanical response are semi-independently tuned; rigorous comparison with particle dispersed and scaffold based hybrids therefore demands standardized reporting of through plane conductivity and τ, t_{Li^+}, internal junction impedance, adhesion energy, symmetric cell critical current density, high voltage stability, and performance under defined stack pressures clarifying how dual skins, ceramic-rich cores, nacre like platelet stacks, and nanofiber interleaves map onto the conductivity modulus stability space relevant to thin Li anodes and high loading cathodes.[89,90]

FUTURE PERSPECTIVES

The transition from liquid electrolytes to HSPEs marks a paradigm shift from empirical trial and error toward deterministic, architecture driven design, where synergy between phase engineered polymer matrices and network engineered inorganic scaffolds governs lithium metal compatibility. To approach the 500 $Wh.kg^{-1}$ benchmark, future research must resolve chemo-mechanical bottlenecks at solid–solid interfaces through hierarchical, 3D ordered architectures that replace stochastic filler dispersions with low τ, deterministic frameworks fabricated via ice templating, co-extrusion or multi material 3D printing. Such structures decouple σ from mechanical modulus, maintaining dendrite suppressing stiffness while achieving room temperature conductivities ≥10^{-3} S cm^{-1}.

Concurrently, next generation HSPEs will adopt Janus or graded designs, transforming monolithic membranes into asymmetric electrolytes tailored to

disparate electrode environments reduction resistant, high modulus anode interfaces and >4.5 V oxidation stable, conformal cathode interfaces for high nickel systems.

This architectural asymmetry will be accelerated by AI and materials genomics: the vast combinatorial space of polymers, salts and fillers is ideally suited for machine learning, utilizing multi scale architecture descriptors such as phase continuity, directional τ and local interfacial area as critical feature inputs. Generative Adversarial Networks (GANs) can utilize these descriptors to design entirely new structural configurations within this combinatorial space while Physics-Informed Neural Networks (PINNs) can evaluate these generated geometries, mapping how specific phase continuities and tortuosities dictate Li ion transport. This enables closed loop laboratories in which physics informed neural networks predict t_{Li^+} and electrochemical windows for virtual candidates that are autonomously synthesized and validated, shifting the field from descriptive screening to prescriptive engineering and targeting $t_{Li^+} \rightarrow 1$.

Commercial translation, however, requires integration with sustainable, high throughput manufacturing moving beyond solvent casting to solvent free routes such as hot melt extrusion, additive manufacturing such as 3D printing for precise spatial control over complex architectures, electrospinning to dictate directional τ through aligned nanofiber templates. Scaled commercial translation will likely rely on solvent free roll to roll (R2R) calendaring to process these hybrid frameworks into dense, ultra-thin films. Furthermore, in situ UV polymerization, the latter enabling injection of liquid pre hybrid precursors that solidify in cell for molecular level conformal contact and reduced interfacial impedance. Scaling to the terawatt hour era further demands "recyclable by design" strategies, including bio derived polymers or vitrimeric networks that permit triggered depolymerization and recovery of high-value ceramic phases. Ultimately, the convergence of deterministic architectural control, AI accelerated discovery, and sustainable manufacturing establishes HSPEs as a leading electrolyte platform for safe, high-energy solid-state lithium batteries.

REFERENCES

1. Antony J.S., Gallant A., Gomez P.L., et al. (2025). Solid-state lithium batteries: Advances, challenges, and future perspectives. *Batteries* **11**:90. DOI:10.3390/batteries11030090
2. Kaviani S. (2025). Covalent organic framework-based solid polymer electrolytes for metal-ion batteries: pioneering the future of DFT, MD, and ML techniques. *Energy Storage Mater.* DOI:10.1016/j.ensm.2025.104671.
3. Sand S.C., Rupp J.L.M., Yildiz B. (2025). A critical review on Li-ion transport, chemistry and structure of ceramic–polymer composite electrolytes for solid state batteries. *Chem. Soc. Rev.* **54**:178–200. DOI:10.1039/d4cs00214h
4. Li Z., Fu J., Zhou X., et al. (2023). Ionic Conduction in Polymer-Based Solid Electrolytes. *Adv. Sci.* 10. DOI:10.1002/advs.202201718.
5. Shamsieva A., Evseev A., Kaviani S., et al. (2025). DFT analysis of furan-based covalent organic framework as electrode materials for lithium and calcium ion batteries. *Comput. Theor. Chem.* DOI:10.1016/j.comptc.2025.115445.
6. Yu X., Chen R., Gan L., et al. (2023). Battery safety: From lithium-ion to solid-state batteries. *Engineering* **21**:9–14. DOI:10.1016/j.eng.2022.08.011
7. Zhao Q., Stalin S., Zhao C.-Z., et al. (2020). Designing solid-state electrolytes for safe, energy-dense batteries. *Nat. Rev. Mater.* **5**:229–252. DOI:10.1038/s41578-019-0165-5
8. Nzereogu P.U., Oyesanya A., Ogba S.N., et al. (2025). Solid-State lithium-ion battery electrolytes: Revolutionizing energy density and safety. *Hybrid Adv.* 8. DOI:10.1016/j.hybadv.2024.100339.
9. Li M., Wang C., Davey K., et al. (2023). Recent progress in electrolyte design for advanced lithium metal batteries. *SmartMat* **4**:e1185. DOI:10.1002/smm2.1185
10. Li Y., Qin Y., Zhao J., et al. (2022). Boosting the ion mobility in solid polymer electrolytes using hollow polymer nanospheres as an additive. *ACS Appl. Mater. Interfaces* **14**:18360–18372. DOI:10.1021/acsami.2c00244
11. Liang H., Wang L., Wang A., et al. (2023). Tailoring practically accessible polymer/inorganic composite electrolytes for all-solid-state lithium metal batteries: a review. *Nano-Micro Lett.* **15**:42. DOI:10.1007/s40820-022-00996-1
12. Muzakir M., Manickavasakam K., Cheng E.J., et al. (2025). Inorganic solid electrolytes for all-solid-state lithium/sodium-ion batteries: recent developments and applications. *J. Mater. Chem. A* **13**:73–135. DOI:10.1039/d4ta06117a
13. Yan S., Yim C.-H., Pankov V., et al. (2021). Perovskite solid-state electrolytes for lithium metal batteries. *Batteries* **7**:75. DOI:10.3390/batteries7040075
14. Kaviani S., Shamsieva A., Piyanzina I., et al. (2025). Enhanced anodic performance of CTF0 monolayer for Li-ion batteries through F and Si co-doping: A DFT insight. *Colloids Surf. A* **705**:135752. DOI:10.1016/j.colsurfa.2024.135752
15. Pan K., Zhang L., Qian W., et al. (2020). A flexible ceramic/polymer hybrid solid electrolyte for solid-state lithium metal batteries. *Adv. Mater.* **32**:2000399. DOI:10.1002/adma.202000399
16. Hu Y., Xie X., Li W., et al. (2023). Recent progress of polymer electrolytes for solid-state lithium batteries. *ACS Sustain. Chem. Eng.* **11**:1253–1277. DOI:10.1021/acssuschemeng.2c05879
17. Dixit M.B., Zaman W., Bootwala Y., et al. (2019). Scalable manufacturing of hybrid solid electrolytes with interface control. *ACS Appl. Mater. Interfaces* **11**:45087–45097. DOI:10.1021/acsami.9b15463
18. Halizan M.Z.M., Kasri M.A., Maliaman N.N., et al. (2025). Integration of solid polymer electrolyte into an efficient and environmentally friendly electrochemical approach in lithium-ion batteries recycling. *J. Energy Storage* **131**:117491. DOI:10.1016/j.est.2025.117491
19. Blatt M.P., Hallinan D.T. (2021). Polymer blend electrolytes for batteries and beyond. *Ind. Eng. Chem. Res.* **60**:17303–17327. DOI:10.1021/acs.iecr.1c02938
20. Wang T., Zhong L., Xiao M., et al. (2023). Block copolymer electrolytes for lithium metal batteries: Strategies to boost both ionic conductivity and mechanical strength. *Prog. Polym. Sci.* **146**:101743. DOI:10.1016/j.progpolymsci.2023.101743
21. Zeng X., Liu X., Zhu H., et al. (2024). Advanced crosslinked solid polymer electrolytes: molecular architecture, strategies, and future perspectives. *Adv. Energy Mater.* **14**:2402671. DOI:10.1002/aenm.202402671
22. Meng N., Zhu X., Lian F. (2022). Particles in composite polymer electrolyte for solid-state lithium batteries: A review. *Particuology* **60**:14–36. DOI:10.1016/j.partic.2021.11.003
23. Yang X., Liu J., Pei N., et al. (2023). The critical role of fillers in composite polymer electrolytes for lithium battery. *Nano-Micro Lett.* **15**:74. DOI:10.1007/s40820-023-01051-3
24. Liao W., Liu C. (2021). Structural Design of Composite Polymer Electrolytes for Solid-state Lithium Metal Batteries. *ChemNanoMat* **7**:1177–1187. DOI:10.1002/cnma.202100382
25. Tian L., Kim J.-W., Kim D.-W. (2024). Solid hybrid electrolytes based on conductive oxides and polymer electrolytes for all-solid-lithium batteries. *Mater. Chem. Front.* **8**:455–484. DOI:10.1039/D3QM00736G
26. Fu J., Li Z., Zhou X., et al. (2022). Ion transport in composite polymer electrolytes. *Mater. Adv.* **3**:3809–3819. DOI:10.1039/D2MA00215A
27. Su Y., Xu F., Zhang X., et al. (2023). Rational design of high-performance PEO/ceramic composite solid electrolytes for lithium metal batteries. *Nano-Micro Lett.* **15**:82. DOI:10.1007/s40820-023-01055-z
28. Kaviani S. (2025). Molecular dynamics and machine learning framework for predicting ion transport and mechanical properties of ionic liquid@ polyvinylidene fluoride gel polymer electrolyte. *J. Ind. Eng. Chem.* DOI:10.1016/j.jiec.2025.11.034.
29. Gao K.W., Loo W.S., Snyder R.L., et al. (2020). Miscible Polyether/Poly (ether–acetal) Electrolyte Blends. *Macromolecules* **53**:5728–5739. DOI:10.1021/acs.macrom.0c01211
30. Li S., Jiang K., Wang J., et al. (2019). Molecular brush with dense PEG side chains: design of a well-defined polymer electrolyte for lithium-ion batteries. *Macromolecules* **52**:7234–7243. DOI:10.1021/acs.macrom.9b01641
31. Caradant L., Verdier N., Foran G., et al. (2021). Extrusion of polymer blend electrolytes for solid-state lithium batteries: a study of polar functional groups. *ACS Appl. Polym. Mater.* **3**:6694–6704. DOI:10.1021/acsapm.1c01393
32. Seiffert S. (2020). Polymer thermodynamics. In: Physical Chemistry of Polymers, De Gruyter, pp:89–128. DOI:10.1515/9783110672817-004.
33. Tsuchida E., Ohno H., Tsunemi K., et al. (1983). Lithium ionic conduction in poly (methacrylic acid)-poly (ethylene oxide) complex containing lithium perchlorate. *Solid State Ion.* **11**:227–233. DOI:10.1016/0167-2738(83)90028-0
34. Sengwa R., Dhatarwal P., Choudhary S. (2014). Role of preparation methods on the structural and dielectric properties of plasticized polymer blend electrolytes: correlation between ionic conductivity and dielectric parameters. *Electrochim. Acta* **142**:359–370. DOI:10.1016/j.electacta.2014.06.135
35. Zhu L., Li J., Jia Y., et al. (2020). Toward high performance solid-state lithium-ion battery with a promising PEO/PPC blend solid polymer electrolyte. *Int. J. Energy Res.* **44**:10168–10178. DOI:10.1002/er.5396
36. Zainal N.F.A., Lai S.A., Chan C.H. (2020). Melt rheological behavior and morphology of poly (ethylene oxide)/natural rubber-graft-poly (methyl methacrylate) blends. *Polymers* **12**:724. DOI:10.3390/polym12030724
37. Galluzzo M.D., Loo W.S., Wang A.A., et al. (2020). Measurement of three transport coefficients and the thermodynamic factor in block copolymer electrolytes with different morphologies. *J. Phys. Chem. B* **124**:921–935. DOI:10.1021/acs.jpcb.9b11066
38. Swann J.M., Topham P.D. (2010). Design and application of nanoscale actuators using block-copolymers. *Polymers* **2**:454–469. DOI:10.3390/polym2020454
39. Butzelaar A.J., Röring P., Hoffmann M., et al. (2021). Advanced block copolymer design for polymer electrolytes: prospects of microphase separation. *Macromolecules* **54**:11101–11112. DOI:10.1021/acs.macrom.1c02147
40. Bergfelt A., Hernández G., Mogensen R., et al. (2020). Mechanically robust yet highly conductive diblock copolymer solid polymer electrolyte for ambient temperature battery applications. *ACS Appl. Polym. Mater.* **2**:939–948. DOI:10.1021/acsapm.9b01142

41. He Y., Liu N., Kohl P.A. (2021). Difunctional block copolymer with ion solvating and crosslinking sites as solid polymer electrolyte for lithium batteries. *J. Power Sources* **481**:228832. DOI:10.1016/j.jpowsour.2020.228832
42. Butzelaar A.J., Roring P., Mach T.P., et al. (2021). Styrene-based poly (ethylene oxide) side-chain block copolymers as solid polymer electrolytes for high-voltage lithium-metal batteries. *ACS Appl. Mater. Interfaces* **13**:39257–39270. DOI:10.1021/acsami.1c08841
43. More S.S., Khupse N.D., Ambekar J.D., et al. (2022). Ionic liquid-supported interpenetrating polymer network flexible solid electrolytes for lithium-ion batteries. *Energy Fuels* **36**:4999–5008. DOI:10.1021/acs.energyfuels.2c01942
44. Lipatov Y., Semenovich G. (1999). The interrelation between the kinetics of the IPN formation at the interface with solid and surface segregation. *Polymer* **40**:6485–6492. DOI:10.1016/S0032-3861(98)00848-9
45. Kailas Kumar R., Duggal H., Samantaray P.K. (2026). Emerging Macromolecular Approaches to Pore Engineering and Interfacial Control Using Interpenetrating Polymer Networks. *Macromol. Rapid Commun.* **47**:e00627. DOI:10.1002/marc.202500627
46. Ha H.-J., Kil E.-H., Kwon Y.H., et al. (2012). UV-curable semi-interpenetrating polymer network-integrated, highly bendable plastic crystal composite electrolytes for shape-conformable all-solid-state lithium ion batteries. *Energy Environ. Sci.* **5**:6491–6499. DOI:10.1039/C2EE03025J
47. Suk J., Lee Y.H., Kim D.W. (2016). Semi-interpenetrating solid polymer electrolyte based on thiol-ene cross-linker for all-solid-state lithium batteries. *J. Power Sources* **334**:154–161. DOI:10.1016/j.jpowsour.2016.09.072
48. Zheng Y., Li X., Li C.Y. (2020). A novel de-coupling solid polymer electrolyte via semi-interpenetrating network for lithium metal battery. *Energy Storage Mater.* **29**:42–51. DOI:10.1016/j.ensm.2020.01.004
49. Homann G., Stolz L., Neuhaus K., et al. (2020). Effective optimization of high voltage solid-state lithium batteries by using poly (ethylene oxide)-based polymer electrolyte with semi-interpenetrating network. *Adv. Funct. Mater.* **30**:2006289. DOI:10.1002/adfm.202006289
50. Zheng Y., Li X., Fullerton W.R., et al. (2021). Interpenetrating network-based hybrid solid and gel electrolytes for high voltage lithium metal batteries. *ACS Appl. Energy Mater.* **4**:5639–5648. DOI:10.1021/acsaem.1c00451
51. Rong Z., Sun Y., Zhao Q., et al. (2022). UV-Cured Semi-Interpenetrating polymer networks of solid electrolytes for rechargeable lithium metal batteries. *Chem. Eng. J.* **437**:135329. DOI:10.1016/j.cej.2022.135329
52. Zeng G., Dai S., Chen X., et al. (2024). Solid-State Graft Polymer Electrolytes with Conductive Backbones and Side Chains for Lithium Batteries. *Macromolecules* **57**:1258–1265. DOI:10.26434/chemrxiv-2023-3fkt9
53. Meng N., Lian F., Cui G. (2021). Macromolecular design of lithium conductive polymer as electrolyte for solid-state lithium batteries. *Small* **17**:2005762. DOI:10.1002/smll.2005762
54. Ji X., Cao M., Fu X., et al. (2020). Efficient room-temperature solid-state lithium ion conductors enabled by mixed-graft block copolymer architectures. *Giant* **3**:100027. DOI:10.1016/j.giant.2020.100027
55. Higa M., Fujino Y., Koumoto T., et al. (2005). All solid-state polymer electrolytes prepared from a hyper-branched graft polymer using atom transfer radical polymerization. *Electrochim. Acta* **50**:3832–3837. DOI:10.1016/j.electacta.2005.02.042
56. Gami P., Das A.K., Vasavan H.N., et al. (2025). PVDF-HFP/PVP-based Miscible Blend Electrolyte for Fast-Charging Lithium Metal Batteries. *Electrochim. Acta* DOI:10.1016/j.electacta.2025.146840.
57. Mei X., Huang Y., Chen S., et al. (2023). Improving Ion Conductivity in Polymer Blend Electrolytes by Tuning Microdynamics and Interfaces. *ACS Appl. Polym. Mater.* **5**:9225–9235. DOI:10.1021/acsapm.3c01658
58. Guo K., Wang J., Shi Z., et al. (2023). One-Step In Situ Polymerization: A Facile Design Strategy for Block Copolymer Electrolytes. *Angew. Chem. Int. Ed.* **62**:e202213606. DOI:10.1002/anie.202213606
59. Song Y.-W., Lee H., Park S.-J., et al. (2023). Advancing Particle Dispersion/Interface Design in Composite Solid Electrolytes for Solid-State Batteries. *J. Phys. Chem. C* **127**:18291–18300. DOI:10.1021/acs.jpcc.3c03889
60. Otani K., Yano T., Akizuki K., et al. (2025). Quantitative Study of Solid Electrolyte Particle Dispersion and Compression Processes in All-Solid-State Batteries Using DEM. *Electrochem.* **93**:063009. DOI:10.5796/electrochemistry.25-71025
61. Chen X., Qiu S., Jian Z., et al. (2025). Designing a self-extinguishing system in a composite electrolyte for highly safe solid-state lithium metal batteries. *ACS Nano* **19**:19297–19309. DOI:10.1021/acsnano.5c01991
62. Lü H., Chen X., Sun Q., et al. (2024). Uniform garnet nanoparticle dispersion in composite polymer electrolytes. *Acta Phys.-Chim. Sin.* **40**:2305016. DOI:10.3866/PKU.WHXB202405016
63. Ho N.X., Dien P.T., Viet C.D., et al. (2025). Silane-assisted dispersion of TiO2 nanoparticles into PEO matrix as ultra-stable composite polymer electrolytes for solid-state lithium batteries. *J. Power Sources* **647**:237205. DOI:10.1016/j.jpowsour.2025.237205
64. Ramkumar B., Aravindan V., Ramasamy H., et al. (2022). Ternary metal oxide filled PEO-based polymer electrolyte for solid-state lithium metal battery: The role of filler particle size. *Solid State Sci.* **132**:106958. DOI:10.1016/j.solidstatesciences.2022.106958
65. Utomo N.W., Hong S., Sinha R., et al. (2024). Solid-state polymer-particle hybrid electrolytes. *Sci. Adv.* **10**:eado4719. DOI:10.1126/sciadv.ado4719
66. Lian H., Liao X., Zhang Y., et al. (2026). Interfacial Molecular Welding via Passivation-Triggered Fluoropolymerization: Boosting Li+ Conduction and Stabilizing Dual Electrode Interfaces. *Adv. Funct. Mater.* DOI:10.1002/adfm.202523355.
67. Ding W.-Q., Lv F., Xu N., et al. (2021). Polyethylene oxide-based solid-state composite polymer electrolytes for rechargeable lithium batteries. *ACS Appl. Energy Mater.* **4**:4581–4601. DOI:10.1021/acsaem.1c00216
68. Sheng O., Jin C., Luo J., et al. (2018). Mg2B2O5 nanowire enabled multifunctional solid-state electrolytes with high ionic conductivity, excellent mechanical properties, and flame-retardant performance. *Nano Lett.* **18**:3104–3112. DOI:10.1021/acs.nanolett.8b01267
69. Song S., Wu Y., Tang W., et al. (2019). Composite solid polymer electrolyte with garnet nanosheets in poly (ethylene oxide). *ACS Sustain. Chem. Eng.* **7**:7163–7170. DOI:10.1021/acssuschemeng.9b00143
70. Zhang D., Meng X., Hou W., et al. (2023). Solid polymer electrolytes: Ion conduction mechanisms and enhancement strategies. *Nano Res. Energy* **2**:e9120050. DOI:10.26599/NRE.2023.9120050
71. Liu X., Xiao Z., Peng H., et al. (2022). Rational Design of LLZO/Polymer Solid Electrolytes for Solid-State Batteries. *Chem.–Asian J.* **17**:e202200929. DOI:10.1002/asia.202200929
72. Li X., Wang J. (2020). One-dimensional and two-dimensional synergized nanostructures for high-performing energy storage and conversion. *InfoMat* **2**:3–32. DOI:10.1002/inf2.12004
73. Wang Z., Li Y., Huang S., et al. (2020). PVD customized 2D porous amorphous silicon nanoflakes percolated with carbon nanotubes for high areal capacity lithium ion batteries. *J. Mater. Chem. A* **8**:4836–4843. DOI:10.1039/c9ta12923e
74. Sahore R., Armstrong B.L., Tang X., et al. (2023). Role of Scaffold Architecture and Excess Surface Polymer Layers in a 3D-Interconnected Ceramic/Polymer Composite Electrolyte. *Adv. Energy Mater.* **13**:2203663. DOI:10.1002/aenm.202203663
75. Li S., Zhang S.Q., Shen L., et al. (2020). Progress and perspective of ceramic/polymer composite solid electrolytes for lithium batteries. *Adv. Sci.* **7**:1903088. DOI:10.1002/advs.201903088
76. He K.Q., Liao X.G., Lian H.J., et al. (2025). Endowing rapid Na+ conduction by architecture design of Na3Zr2Si2PO12 in composite electrolytes for ultralong lifespan quasi-solid-state sodium metal batteries. *Rare Met.* **44**:3795–3805. DOI:10.1007/s12598-024-03213-7
77. Chen Q., Ouyang C., Liang Y., et al. (2024). Composite polymer electrolyte with vertically aligned garnet scaffolds for quasi solid-state lithium batteries. *Energy Storage Mater.* **69**:103418. DOI:10.1016/j.ensm.2024.103418
78. Wang R., Dong Q., Wang C., et al. (2021). High-temperature ultrafast sintering: exploiting a new kinetic region to fabricate porous solid-state electrolyte scaffolds. *Adv. Mater.* **33**:2100726. DOI:10.1002/adma.202100726
79. Wei B., Li Y., Lin W., et al. (2024). A wrapped and infiltrated~ 20-μm-thick 3D ceramic framework composite enables fast Li+ diffusion and interfacial compatibility for lithium-metal batteries. *Compos. Part B Eng.* **272**:111192. DOI:10.1016/j.compositesb.2024.111192
80. Song S., Qin X., Ruan Y., et al. (2020). Enhanced performance of solid-state lithium-air batteries with continuous 3D garnet network added composite polymer electrolyte. *J. Power Sources* **461**:228146. DOI:10.1016/j.jpowsour.2020.228146
81. Duan H., Yin Y.-X., Shi Y., et al. (2018). Dendrite-free Li-metal battery enabled by a thin asymmetric solid electrolyte with engineered layers. *J. Am. Chem. Soc.* **140**:82–85. DOI:10.1021/jacs.7b10864
82. Yu X., Li J., Manthiram A. (2020). Rational design of a laminated dual-polymer/polymer–ceramic composite electrolyte for high-voltage all-solid-state lithium batteries. *ACS Mater. Lett.* **2**:317–324. DOI:10.1021/acsmaterialslett.9b00535
83. Li A., Liao X., Zhang H., et al. (2020). Nacre-inspired composite electrolytes for load-bearing solid-state lithium-metal batteries. *Adv. Mater.* **32**:1905517. DOI:10.1002/adma.201905517
84. Zhang N., Wu S., Zheng H., et al. (2023). Recent progress of multilayer polymer electrolytes for lithium batteries. *Energy Mater.* DOI:10.20517/energymater.2022.64.
85. Yuan Y., Wang B., Xue K., et al. (2023). High-voltage solid-state lithium metal batteries with stable anodic and cathodic interfaces by a laminated solid polymer electrolyte. *ACS Appl. Mater. Interfaces* **15**:17144–17151. DOI:10.1021/acsami.2c23058
86. Li B., Su Q., Yu L., et al. (2021). Ultrathin, flexible, and sandwiched structure composite polymer electrolyte membrane for solid-state lithium batteries. *J. Membr. Sci.* **618**:118734. DOI:10.1016/j.memsci.2020.118734
87. Tian L., Liu Y., Su Z., et al. (2021). A lithiated organic nanofiber-reinforced composite polymer electrolyte enabling Li-ion conduction highways for solid-state lithium metal batteries. *J. Mater. Chem. A* **9**:23882–23890. DOI:10.1039/D1TA06269G
88. Fu Y., Chen Y., Yu X., et al. (2022). Fiber metal laminated structural batteries with multifunctional solid polymer electrolytes. *Compos. Sci. Technol.* **230**:109731. DOI:10.1016/j.compscitech.2022.109731
89. Sun J., Gargitter V., Pei S., et al. (2020). Mechanical and electrochemical

performance of hybrid laminated structural composites with carbon fiber/solid electrolyte supercapacitor interleaves. *Compos. Sci. Technol.* **196**:108234. DOI:10.1016/j.compscitech.2020.108234
90. Yu X., Xue L., Goodenough J.B., et al. (2021). Ambient-temperature all-solid-state sodium batteries with a laminated composite electrolyte. *Adv. Funct. Mater.* **31**:2002144. DOI:10.1002/adfm.202002144
91. Didwal P.N., Singhbabu Y., Verma R., et al. (2021). An advanced solid polymer electrolyte composed of poly (propylene carbonate) and mesoporous silica nanoparticles for all-solid-state lithium-ion batteries. *Energy Storage Mater.* **37**:476–490. DOI:10.1016/j.ensm.2021.03.026
92. Zhang Y., Wang X., Feng W., et al. (2019). The effects of the size and content of BaTiO3 nanoparticles on solid polymer electrolytes for all-solid-state lithium-ion batteries. *J. Solid State Electrochem.* **23**:749–758. DOI:10.1007/s10008-018-04175-4
93. Raj A., Grignard B., Bourguignon M., et al. (2025). Composite Polymer Electrolytes Based on Silicon Dioxide Nanoparticles for Lithium Metal Batteries. *Macromol. Chem. Phys.* **226**:e00242. DOI:10.1002/macp.202500242
94. Yang T., Zheng J., Cheng Q., et al. (2017). Composite polymer electrolytes with Li7La3Zr2O12 garnet-type nanowires as ceramic fillers: mechanism of conductivity enhancement and role of doping and morphology. *ACS Appl. Mater. Interfaces* **9**:21773–21780. DOI:10.1021/acsami.7b05622
95. Li Y., Zhang W., Dou Q., et al. (2019). Li7La3Zr2O12 ceramic nanofiber-incorporated composite polymer electrolytes for lithium metal batteries. *J. Mater. Chem. A* **7**:3391–3398. DOI:10.1039/C8TA11449H
96. Liu W., Liu N., Sun J., et al. (2015). Ionic conductivity enhancement of polymer electrolytes with ceramic nanowire fillers. *Nano Lett.* **15**:2740–2745. DOI:10.1021/acs.nanolett.5b00600
97. Liu W., Lee S.W., Lin D., et al. (2017). Enhancing ionic conductivity in composite polymer electrolytes with well-aligned ceramic nanowires. *Nat. Energy* **2**:1–7. DOI:10.1038/nenergy.2017.112
98. Zhai H., Xu P., Ning M., et al. (2017). A flexible solid composite electrolyte with vertically aligned and connected ion-conducting nanoparticles for lithium batteries. *Nano Lett.* **17**:3182–3187. DOI:10.1021/acs.nanolett.7b00715
99. Zheng X., Wei J., Lin W., et al. (2022). Bridging Li7La3Zr2O12 nanofibers with Poly (ethylene oxide) by coordination bonds to enhance the cycling stability of all-solid-state lithium metal batteries. *ACS Appl. Mater. Interfaces* **14**:5346–5354. DOI:10.1021/acsami.1c21131
100. Wang J., Guo S., Li Z., et al. (2022). Highly conductive thin composite solid electrolyte with vertical Li7La3Zr2O12 sheet arrays for high-energy-density all-solid-state lithium battery. *Chem. Eng. J.* **450**:137994. DOI:10.1016/j.cej.2022.137994
101. Zhao Y., Yan J., Cai W., et al. (2019). Elastic and well-aligned ceramic LLZO nanofiber based electrolytes for solid-state lithium batteries. *Energy Storage Mater.* **23**:306–313. DOI:10.1016/j.ensm.2019.02.016
102. Feng T., Hu Y., Xu L., et al. (2022). Improving the cyclability of solid polymer electrolyte with porous V2O5 nanotube filler. *Mater. Today Energy* **28**:101062. DOI:10.1016/j.mtener.2022.101062
103. Li Y., Sun Z., Liu D., et al. (2020). A composite solid polymer electrolyte incorporating MnO 2 nanosheets with reinforced mechanical properties and electrochemical stability for lithium metal batteries. *J. Mater. Chem. A* **8**:2021–2032. DOI:10.1039/c9ta11542k
104. Ao X., Wang X., Tan J., et al. (2021). Nanocomposite with fast Li+ conducting percolation network: Solid polymer electrolyte with Li+ non-conducting filler. *Nano Energy* **79**:105475. DOI:10.1016/j.nanoen.2020.105475
105. Guo S., Kou W., Wu W., et al. (2022). Thin laminar inorganic solid electrolyte with high ionic conductance towards high-performance all-solid-state lithium battery. *Chem. Eng. J.* **427**:131948. DOI:10.1016/j.cej.2021.131948
106. Cheng J., Hou G., Chen Q., et al. (2022). Sheet-like garnet structure design for upgrading PEO-based electrolyte. *Chem. Eng. J.* **429**:132343. DOI:10.1016/j.cej.2021.132343
107. Bae J., Li Y., Zhang J., et al. (2018). A 3D nanostructured hydrogel-framework-derived high-performance composite polymer lithium-ion electrolyte. *Angew. Chem. Int. Ed.* **57**:2096–2100. DOI:10.1002/anie.201710841
108. Zekoll S., Marriner-Edwards C., Hekselman A.O., et al. (2018). Hybrid electrolytes with 3D bicontinuous ordered ceramic and polymer microchannels for all-solid-state batteries. *Energy Environ. Sci.* **11**:185–201. DOI:10.1039/C7EE02723K
109. Pan P., Zhang M., Cheng Z., et al. (2022). Garnet ceramic fabric-reinforced flexible composite solid electrolyte derived from silk template for safe and long-term stable All-Solid-State lithium metal batteries. *Energy Storage Mater.* **47**:279–287. DOI:10.1016/j.ensm.2022.01.047
110. Wang G., Liu H., Liang Y., et al. (2022). Composite polymer electrolyte with three-dimensional ion transport channels constructed by NaCl template for solid-state lithium metal batteries. *Energy Storage Mater.* **45**:1212–1219. DOI:10.1016/j.ensm.2022.01.039
111. Tian L.W., Kim J.W., Hong S.-B., et al. (2022). All-solid-state lithium batteries featuring hybrid electrolytes based on Li7La3Zr2O12 framework and full-concentration gradient Ni-rich NCM cathode. *Chem. Eng. J.* **450**:138043. DOI:10.1016/j.cej.2022.138043
112. Bae J., Li Y., Zhao F., et al. (2018). Designing 3D nanostructured garnet frameworks for enhancing ionic conductivity and flexibility in composite polymer electrolytes for lithium batteries. *Energy Storage Mater.* **15**:46–52. DOI:10.1016/j.ensm.2018.01.005
113. Liu S., Zhao Y., Li X., et al. (2021). Solid-state lithium metal batteries with extended cycling enabled by dynamic adaptive solid-state interfaces. *Adv. Mater.* **33**:2008084. DOI:10.1002/adma.2008084

FUNDING AND ACKNOWLEDGMENTS

This research has received funding support from the NSRF via the Research and Innovation Acceleration Agency for Competitiveness and Area Development (RCAD) (Program Management Unit for Frontier Brainpower and Future Industries) [grant number B42G690095]) and the Thailand Science Research and Innovation Fund Chulalongkorn University (INDFF691442300035). Anagipura Tharika Gimhani would like to thank Chulalongkorn University in Thailand for their ASEAN/NON-ASEAN scholarship sponsorship.

AUTHOR CONTRIBUTIONS

All authors reviewed and proved the manuscript.

DECLARATION OF INTERESTS

The authors declare no competing interests.

DATA AND CODE AVAILABILITY

Data are available from the corresponding author upon reasonable request.